



One-pot di- and polysaccharides conversion to highly selective 2,5-dimethylfuran over Cu-Pd/Amino-functionalized Zr-based metal-organic framework (UiO-66(NH₂))@SGO tandem catalyst

Rizki Insyani^a, Deepak Verma^{a,d,e}, Handi Setiadi Cahyadi^a, Seung Min Kim^b, Seok Ki Kim^c, Neha Karanwal^a, Jaehoon Kim^{a,d,e,*}

^a SKKU Advanced Institute of Nanotechnology (SAINT), Sungkyunkwan University, 2066 Seobu-Ro, Jangan-Gu, Suwon, Gyeong Gi-Do, 16419, Republic of Korea

^b Institute of Advanced Composite Materials, Korea Institute of Science and Technology, Chudong-ro 92, Bongdong-eup, Wanju-gun, Jeonranbuk-do, Republic of Korea

^c Carbon Resource Institute, Korea Research Institute of Chemical Technology, 141 Gajeongro, Yuseong, Daejeon 34114, Republic of Korea

^d School of Mechanical Engineering, Sungkyunkwan University, 2066 Seobu-Ro, Jangan-Gu, Suwon, Gyeong Gi-Do, 16419, Republic of Korea

^e School of Chemical Engineering, Sungkyunkwan University, 2066 Seobu-Ro, Jangan-Gu, Suwon, Gyeong Gi-Do, 16419, Republic of Korea

ARTICLE INFO

Keywords:

2,5-Dimethylfuran
Disaccharide
Direct conversion
Tandem catalyst
UiO-66(NH₂)

ABSTRACT

Tandem heterogenous catalysis of bimetallic Cu-Pd on UiO-66(NH₂) that were incorporated into sulfonated graphene oxide (Cu-Pd/UiO-66(NH₂))@SGO or Cu-Pd/US) was investigated for the one-pot, direct conversion of di- and polysaccharides into 2,5-dimethylfuran (2,5-DMF) without separation of reaction intermediates. In the absence of a homogeneous acidic catalyst, consecutive reactions of glycosidic bond cleavage, isomerization, dehydration, and hydrogenation/hydrogenolysis were preceded by the synergistic effect of a multifunctional Cu-Pd/US catalyst. The strength and ratio of Brønsted and Lewis acid sites by adjusting UiO-66(NH₂) to SGO ratios resulted in high-yield 5-(hydroxymethyl)furfural (5-HMF) through sequential glycosidic bond cleavage, isomerization, and dehydration of sucrose. Unlike monometallic Cu and Pd, bimetallic Cu-Pd promoted consecutive C–OH hydrogenolysis and C=O hydrogenation of reaction intermediates, producing 2,5-DMF with a high yield of 73.4% during the one-pot conversion of sucrose at 200 °C and 1 MPa H₂ for 3 h. When starch was converted over Cu-Pd/US, 2,5-DMF was formed with 53.6% yield. Direct cellulose conversion into 2,5-DMF with a yield of 29.8% was achieved in the presence of 0.01 M HCl and Cu-Pd/US. The presence of the amino functional group (–NH₂) in the UiO-66 framework was beneficial for improving the feed conversion and maintaining catalyst recyclability up to five times with almost no activity loss.

1. Introduction

Conversion of natural biomass into targeted valuable chemicals requires consecutive multi-step reactions and separation/purification of reaction intermediates. This makes the whole process time-consuming, uneconomical, and energy-intensive. Therefore, the one-pot, direct conversion of biomass into value-added chemicals is highly desirable because the production of an unstable reaction intermediate (e.g., 5-(hydroxymethyl)furfural (5-HMF), furfural, and levulinic acid) [1] can be circumvented, side reactions can be suppressed [2], and chemical wastes can be minimized during separation/purification. In this regard, it is critical to design an effective multifunctional tandem catalyst that can lead to desirable consecutive reaction pathways for achieving high-yield and highly selective targeted final products.

As a biofuel alternative, 2,5-dimethylfuran (2,5-DMF) has a great potential in a wide range of applications in transportation sectors [3,4]. 2,5-DMF can also be used as a precursor for producing chemicals used in semiconductor manufacturing, pharmaceutical industries, and engineering polymers, as shown in Scheme 1. For example, 2,5-DMF can be used as a substrate for the synthesis of pentacene through a Diels-Alder reaction with maleic anhydride to produce 3,6-dimethylphthalic anhydride, which can be used as an organic semiconductor [5,6]. In addition, 2,5-DMF can be used as a precursor in a Paal-Knorr reaction to produce pyrroles, which are primarily used to synthesis drug intermediates [7]. Recently, versatile routes for utilizing 2,5-DMF to produce *p*-xylene through a Diels-Alder reaction with ethylene [8] or ethanol [9] have been proposed. Further oxidation of *p*-xylene through Amoco, Mitsubishi, Eastman, and Henkel processes has been well-

* Corresponding author at: School of Mechanical Engineering, School of Chemical Engineering and SKKU Advanced Institute of Nanotechnology (SAINT), Sungkyunkwan University, 2066 Seobu-Ro, Jangan-Gu, Gyeong Gi-Do, Suwon, 16419, Republic of Korea.

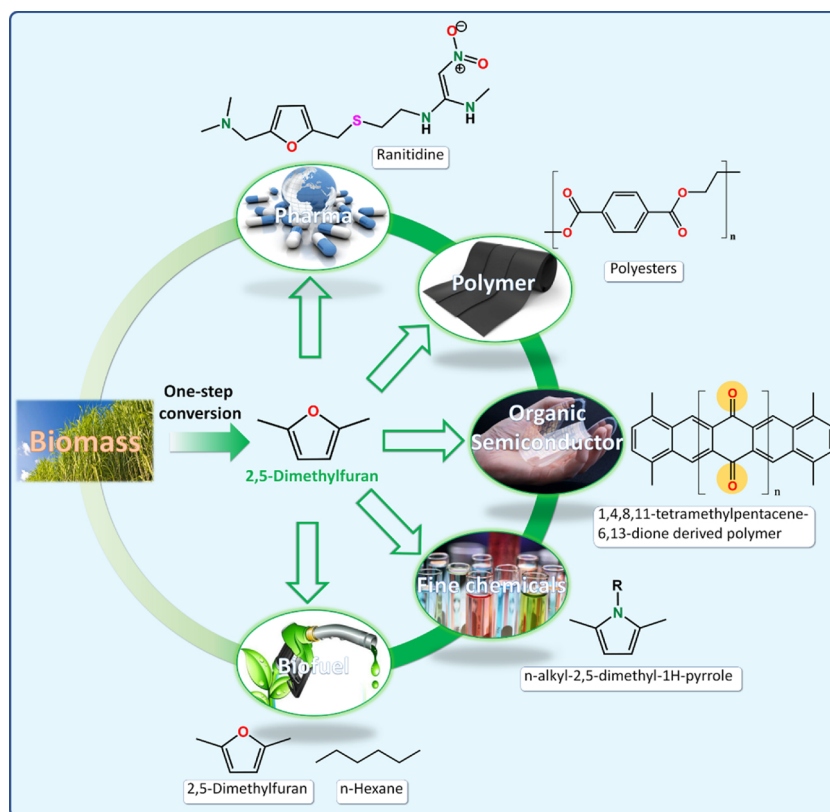
E-mail address: jaehoonkim@skku.edu (J. Kim).

<https://doi.org/10.1016/j.apcatb.2018.10.036>

Received 18 June 2018; Received in revised form 17 September 2018; Accepted 16 October 2018

Available online 21 October 2018

0926-3373/ © 2018 Elsevier B.V. All rights reserved.



Scheme 1. Potential application of 2,5-DMF in chemical industries.

established to produce terephthalic acid, which is a well-known monomer in polymer industries. Recent studies have demonstrated that upgrading 2,5-DMF can produce linear oxygenates (hexanol and hexanone) [10] and 2,5-dimethyltetrahydrofuran (DMTHF) [11], which are highly useful in the fragrance and solvent industries, respectively.

In spite of the numerous potential applications of 2,5-DMF as a fuel and a platform chemical, the one-pot, direct production of 2,5-DMF from monosaccharides (fructose and glucose) is still a great challenge. Most previous approaches involved multi-step reactions and purifications when producing high-yield 2,5-DMF, for example, dehydration of fructose to 5-HMF over acidic sites, purification of 5-HMF, and hydrogenolysis of 5-HMF to 2,5-DMF over metal sites [12,13]. When fructose was used as the feedstock and the produced 5-HMF was properly purified, 2,5-DMF was produced with high yield (70–99%) [4,14], while the use of unpurified 5-HMF decreased the 2,5-DMF yield significantly (9–41%) via heterogeneous catalysis [15]. The combined use of homogeneous Lewis acid catalysts (e.g. ZnCl_2 , AlCl_3) and noble metal supported heterogeneous catalysts (e.g. Pd/C , Ru/C) could directly convert fructose into 2,5-DMF with yields of 22–66% [16,17]. Recently, fructose conversion over $\text{Pd/C-SO}_3\text{H}$ modified with trimethylchlorosilane resulted in a high 2,5-DMF yield of 88% [18]. In our previous work, we presented the one-pot conversion of fructose over a Pd/Zr -based metal–organic framework@ sulfonated graphene oxide (Pd/Uio-66@SGO), which retained both the acid and hydrogenation sites, and could produce high-yield 2,5-DMF (70.5%) [12]. On the other hand, when glucose was used as a feedstock, which requires additional isomerization of fructose, 2,5-DMF was directly produced with 45% yield over the Pd/Uio-66@SGO catalyst. The previous work demonstrated that the one-pot conversion of monosaccharides over multifunctional catalysts could be a promising approach for producing 2,5-DMF. However, the direct one-pot conversion of disaccharides (e.g., sucrose, cellobiose) and polysaccharides (e.g., starch, cellulose) into 2,5-DMF in the presence of a heterogeneous catalyst and consecutive reaction mechanisms have been rarely examined (see Table S1). A typical method to produce fructose is

the enzymatic hydrolysis of cellulose and enzymatic isomerization of glucose. However, the huge amounts of expensive enzymes required to ensure high throughput of glucose and fructose and the narrow isomerization processing window could increase the overall production cost [19]. Therefore, it is highly desirable to develop an efficient pathway for producing 2,5-DMF directly from polysaccharides.

Herein, we aimed to produce 2,5-DMF directly from polysaccharide (starch, cellulose), disaccharides (sucrose, cellobiose), and monosaccharides (glucose and fructose) using a multifunctional Cu-Pd /amino-functionalized Zr -based metal-organic framework ($\text{UiO-66}(\text{NH}_2)\text{@sulfonated graphene oxide tandem catalyst}$ ($\text{Cu-Pd/UiO-66}(\text{NH}_2)\text{@SGO}$). To achieve the goal of direct polysaccharide conversion into 2,5-DMF, it is essential to design a new multifunctional catalyst to precede consecutive series of reactions: (1) glycosidic bond cleavage of polysaccharide over Brønsted acid site to produce glucose, (2) isomerization of glucose over Lewis acid sites to produce fructose, (3) dehydration of fructose to produce 5-HMF over Brønsted acid site, and (4) hydrogenolysis/hydrogenation of 5-HMF over metallic active sites to produce 2,5-DMF. Herein, to isomerize glycosidic bond cleavage, Brønsted and Lewis acid sites were carefully controlled by adjusting the $\text{UiO-66}(\text{NH}_2)$ to SGO ratio. In addition, the composition of bimetallic Cu-Pd phases was controlled to enhance hydrogenolysis/hydrogenation activity of 5-HMF while suppressing side reactions, such as over-hydrogenation, ring saturation, and ring opening. Finally, the relationship between the catalyst properties and their performance was investigated in order to understand consecutive reaction pathways of the glycosidic bond cleavage, isomerization, dehydration, and hydrogenolysis/hydrogenation.

2. Experimental method

2.1. Materials

Zirconium chloride (ZrCl_4 , $\geq 99.5\%$), 2-aminoterephthalic acid (99%), copper(II) nitrate hemi(pentahydrate) ($\text{Cu}(\text{NO}_3)_2 \cdot 2.5\text{H}_2\text{O}$,

$\geq 99.9\%$), hydrazine monohydrate ($\text{N}_2\text{H}_4\cdot\text{H}_2\text{O}$, $> 98\%$), starch (from potato), sucrose (99%), cellobiose ($\geq 98\%$), *d*-fructose (99%), 2,5-dimethylfuran (2,5-DMF, $> 98\%$), and furfural (FA, $> 98\%$) were purchased from Thermo Fisher Scientific (USA). Graphite powder ($< 45\ \mu\text{m}$, $> 99.99\%$), potassium permanganate (KMnO_4 , $\geq 99.0\%$), palladium chloride (PdCl_2 , $> 99\%$), sulfuric acid (H_2SO_4 , 98%), sodium hydroxide (NaOH , $\geq 97.0\%$, pellets), *d*-glucose ($> 99\%$), 5-hydroxymethylfurfural (5-HMF, analytical standard), 5-methylfurfural (5-MFA, analytical standard), and cellulose (microcrystalline, powder) were purchased from Sigma Aldrich (USA). Hydrochloric acid (HCl , 35%), phosphoric acid (H_3PO_4 , 85%), sodium nitrate (NaNO_3 , 99%), *N,N*-dimethylformamide (*N,N*-DMF, 99.9%), and tetrahydrofuran (THF, 99%) were purchased from Daejung Chemical (South Korea). All chemicals were used as received without further purification. Distilled and deionized (DDI) water was prepared using an AQUAMax™-Basic 363 water purification system (Younglin Instrument Co., Ltd., South Korea).

2.2. Catalyst preparation

2.2.1. Synthesis of sulfonated graphene oxide (SGO)

Sulfonated graphene oxide (SGO) was synthesized according to a previously reported method [20,21]. Typically, a 400 mL acid solution mixture of $\text{H}_2\text{SO}_4\text{:H}_3\text{PO}_4$ (9:1 by v/v) was added to 30 g graphite, and the whole solution was thoroughly mixed. After the temperature of the mixture decreased to 0°C , 18 g KMnO_4 was slowly and carefully added into the graphite-acid mixture. The mixture was then heated at 50°C for 12 h and cooled down to 20°C . A further oxidation step was conducted by first transferring the mixture to a 1 L bottle containing 400 mL iced-DDI water, and 3 mL of 30 wt% aqueous H_2O_2 solution was subsequently added drop-wise. The yellow precipitate was obtained after complete oxidation and was settled overnight at room temperature. The produced SGO was then centrifuged from the acid solution at 4000 rpm for 30 min at 4°C . The solid was then washed with 400 mL DDI water, 400 mL HCl , and 400 mL ethanol to remove residual chemicals. Furthermore, SGO was filtered and dried overnight at 80°C in vacuum conditions.

2.2.2. Synthesis of amino-functionalized-UiO-66 ($\text{UiO-66}(\text{NH}_2)$)

Amino-functionalized-UiO-66, which was denoted as $\text{UiO-66}(\text{NH}_2)$, was synthesized according to a previously reported method [22]. Typically, 0.63 g of ZrCl_4 (2.7 mmol) and 5 mL of 35% HCl aqueous solution were mixed and dissolved in 25 mL of *N,N*-DMF by ultrasonication for 30 min. Then, 0.62 g of 2-amino terephthalic acid (3.75 mmol) dissolved in 50 mL of *N,N*-DMF was added to the former solution of ZrCl_4 and HCl , and the whole solution was further sonicated for the next 30 min to obtain a clear transparent solution. The solution was then held overnight at 80°C in a convection oven. The yellow precipitate formed as a result of $\text{UiO-66}(\text{NH}_2)$ crystallization, was recovered by vacuum filtration at room temperature, and was subsequently washed at least three times with 20 mL of *N,N*-DMF and 150 mL of ethanol to remove the unreacted ligand. The washed product was vacuum-dried overnight at 80°C . Prior to metal loading, $\text{UiO-66}(\text{NH}_2)$ was dispersed in methanol, sonicated for 5 min, and then dried at 150°C for 2 h to remove the residual solvents and to activate the support.

2.2.3. Synthesis of $M/\text{UiO-66}(\text{NH}_2)\text{@SGO}$ catalyst ($M = \text{Cu}$, Pd , or Cu-Pd)

For the synthesis of 1 g of 10 wt% Cu loaded on $\text{UiO-66}(\text{NH}_2)\text{@SGO}$ (hereafter designated as 10Cu/US), 0.366 g of $\text{Cu}(\text{NO}_3)_2\cdot 2.5\text{H}_2\text{O}$ was dissolved in 10 mL of ethanol. Then 0.45 g of pre-activated $\text{UiO-66}(\text{NH}_2)$ was added to the Cu^{2+} -ethanol solution, and the whole solution was sonicated for 5 min and stirred for 2 h. Metal reduction was conducted by adding 500 μL $\text{N}_2\text{H}_4\cdot\text{H}_2\text{O}$ dissolved in 10 mL of ethanol drop-wise to the Cu^{2+} and $\text{UiO-66}(\text{NH}_2)$ solution. To complete the reduction of Cu^{2+} to Cu^0 , the solution mixture was stirred overnight at

room temperature. The color of the solution mixture changed from blue to grey, indicating that Cu^{2+} was reduced on the surface of $\text{UiO-66}(\text{NH}_2)$. The Cu reduction method using hydrazine hydrate ($\text{N}_2\text{H}_4\cdot\text{H}_2\text{O}$) has been reported previously [23]. Next, 0.45 g of SGO dispersed in 10 mL of ethanol was added to the $\text{Cu}/\text{UiO-66}(\text{NH}_2)$ ethanol solution, and the entire solution was stirred for 2 h. The synthesized $\text{Cu}/\text{UiO-66}(\text{NH}_2)\text{@SGO}$ was filtered and washed with 50 mL of ethanol and vacuum-dried overnight at 80°C . In the formation of $\text{Cu}/\text{UiO-66}(\text{NH}_2)\text{@SGO}$, approximately 10 wt% Cu was loaded based on the weight of $\text{UiO-66}(\text{NH}_2)\text{@SGO}$. The Cu loading was controlled by adjusting the amount of $\text{Cu}(\text{NO}_3)_2\cdot 2.5\text{H}_2\text{O}$ dissolved in ethanol. To synthesize 2 wt% Pd loaded on $\text{UiO-66}(\text{NH}_2)\text{@SGO}$, 0.0166 g of PdCl_2 was dissolved in 10 mL ethanol, and the final procedure is the same as that was used to synthesize 10Cu/US. The synthesized $\text{Pd}/\text{UiO-66}(\text{NH}_2)\text{@SGO}$ was denoted as 2Pd/US.

To synthesize the bimetallic $\text{Cu-Pd}/\text{UiO-66}(\text{NH}_2)\text{@SGO}$ catalysts with various Pd loadings, 0.366 g $\text{Cu}(\text{NO}_3)_2\cdot 2.5\text{H}_2\text{O}$ and an experimentally desired amount of PdCl_2 were dissolved separately in 10 mL ethanol. After complete solvation, the Cu^{2+} solution and the Pd^{2+} solution were mixed and stirred for further homogenization. Then, 0.445 g of the pre-activated- $\text{UiO-66}(\text{NH}_2)$ was added to the Cu^{2+} and Pd^{2+} -ethanol solution, and the solution was sonicated for 5 min and stirred for 2 h. The Cu-Pd reduction and incorporation of SGO to $\text{Cu-Pd}/\text{UiO-66}(\text{NH}_2)$ were carried out using the same method that was used to synthesize 10Cu/US. The formed $\text{Cu-Pd}/\text{UiO-66}(\text{NH}_2)\text{@SGO}$ catalyst was denoted as 10Cu- \mathcal{X} Pd/US ($\mathcal{X} = 0.5, 1.0, 2.0$ wt%, Pd loading based on the weight of $\text{UiO-66}(\text{NH}_2)\text{@SGO}$).

2.3. Reaction

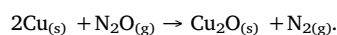
The conversion of monosaccharides (fructose and glucose), disaccharides (sucrose and cellobiose), and polysaccharides (starch and cellulose) were performed in a custom-built SUS 316 batch reactor with an inner volume of 140 mL. The reactor was equipped with a mechanically driven agitator, thermocouples, and inlet and outlet gas purge lines. A detailed description of the reactor system is given elsewhere [24]. Typically, 1 mmol of feed and experimentally desired amount of catalyst were added to the reactor chamber and mixed with 40 mL of THF. The reactor was tightly sealed and purged three times with H_2 to remove air. Then the reactor was pressurized with H_2 at 1 MPa, and the reaction proceeded at various temperatures and times. After the reaction finished, cold-water quenching was applied to the reactor to stop the reaction. A small amount of liquid sample (~ 1 mL) was collected for the product yield analysis. The products in the reactor were then collected and the liquid product was separated from the solid residue (if formed) and the catalyst by filtration. The solid residue and the used-catalyst were washed with acetone and methanol. The remaining solid residue and the catalyst were then dried in a vacuum oven at 105°C overnight to calculate the feed conversion. For catalyst recyclability tests, the used catalyst was further washed with 50 mL of DDI water at 40°C to dissolve any unconverted sugars. The washed catalyst was then dried in a vacuum oven overnight at 105°C before being used in the next cycle.

2.4. Characterization of catalyst

X-ray diffraction (XRD) patterns were collected using a high-power powder X-ray diffractometer system (D8 Advance, Bruker Corporation, Germany). The spectra were recorded at 2θ values ranging from 3° to 90° (scanning speed of 0.02° per second) by a Lynxeye detector coupled to an X-ray generator tube setting at $\text{Cu-K}\alpha$ ($\lambda = 1.5418\ \text{\AA}$) and Ni foil- $\text{K}\beta$ filtered radiation at 40 kV and 20 mA. X-ray photoelectron spectroscopy (XPS) measurements were performed by ESCALAB 250Xi equipped with a twin-crystal microfocusing monochromator used as an X-ray monochromator and Al $\text{K}\alpha$ anode radiation as the excitation source (ThermoFisher Scientific, UK). Cu and Pd metal contents in the catalyst

composite were quantitatively determined using inductively coupled plasma-optical emission spectroscopy (ICP-OES, Varian Model 730-ES, USA). The textural properties of the catalysts, including N_2 adsorption-desorption behavior at 77 K, surface area, and pore size distribution, were studied by the Brunauer–Emmett–Teller (BET) method, which was performed using a Belsorp-mini II apparatus (BEL Inc., Japan). All the catalyst samples were pretreated to evacuate trapped moisture and residual solvent at 150 °C for 12 h using BELPREP–vac II (BEL Inc.) equipment prior to measurement. The morphologies and microstructures of the catalyst samples were investigated using a JSM7000F field-emission scanning electron microscope (FE-SEM, JEOL, Japan) equipped with an energy dispersive X-ray spectrometer (EDS) and an aberration-corrected high-resolution transmission electron microscope (HR-TEM, Titan Cubed G² 60–300, FEI Co. Ltd., USA) operated at an accelerating voltage of 80 kV. High-angle annular dark-field scanning transmission electron microscopy (HAADF-STEM) was performed using JEM-3010 with an electron acceleration energy of 300 keV and a spatial resolution of 1.4 Å (JEOL, Japan). The surface acidity of the catalyst was measured by potentiometric titration and pyridine-Fourier transform infrared (Py-FTIR) spectroscopy. The proton concentration in UiO-66(NH₂)@SGO was determined by acid-base potentiometric titration, which was conducted using a ThermoScientific™ Orion™ Star A211 pH benchtop meter. The pH meter was calibrated using pH buffer solutions of 4.00, 7.00, and 10.01 with accuracy 99.4% determined by linear regression. Typically, 60 mL of 0.01 M NaNO₃ was added to 50 mg of catalyst in vials. The mixture was then stirred for 18 h to ensure the equilibrium ion-exchange reagent released the acidic protons from UiO-66(NH₂) into the aqueous solution. The mixture was then centrifuged to separate the supernatant and solid phases. Prior to titration, the pH of the supernatant was adjusted to 3.00 by adding 0.1 M HCl. The supernatant was then titrated with a standardized 0.01 M NaOH until a pH value of 10–11 was achieved. The titration curve was plotted to obtain the end-point equivalent. Py-FTIR was used to further investigate the acidity and acid sites in the catalysts. The IR spectra were recorded in the 1400–1700 cm^{−1} range at a resolution of 4 cm^{−1} using a Thermo Nicolet 4700 apparatus. Approximately 30 mg of each catalyst was pressed to form self-standing wafers. The wafer sample was then pretreated at 200 °C with He flowing at 20 sccm for 1 h prior to pyridine adsorption. The pyridine adsorption was performed by flowing pyridine-vapor-saturated He into the cell at 150 °C for 20 min. Then, the cell was purged with pure He at 200 °C for 3 h to remove physically adsorbed pyridine. A total of 32 scans were performed for each sample, and the FTIR spectra of the sample were recorded at room temperature in absorbance mode. The amount of Brønsted and Lewis acid sites of the catalysts was estimated by a peak area curve-fitting method (deconvolution) of the IR bands in the 1600–1400 cm^{−1} range using the Pearson VII model (which is flexible for both Lorentzian and Gaussian functions). The corresponding approach has been previously reported for the spectral analysis of proton site distribution in zeolite [25]. To investigate the thermal stability and decomposition behavior of UiO-66(NH₂) and UiO-66(NH₂)@SGO, the samples were analyzed using a Q50 thermogravimetric analyzer (TGA, TA Instruments, USA) under an air flow condition at temperatures ranging from 30 to 800 °C with a heating rate of 10 °C min^{−1} and a flow rate of 60 mL min^{−1}. The hydrogen temperature-programmed reduction (H₂-TPR) experiments were carried out using a BELCAT temperature program analyzer to assess the reduction properties of the metal sites in UiO-66(NH₂)@SGO. Approximately 0.05 g of the catalyst was loaded into a sample tube and thermally treated under an Ar gas stream at 250 °C for 1 h to remove physisorbed water and other gaseous impurities. The sample was then cooled to room temperature under Ar gas. The pretreated sample was heated to 250 °C with a 10 °C min^{−1} heating rate under a 5% H₂/Ar flow at 30 mL min^{−1}. The H₂ consumption was detected by a thermal conductivity detector (TCD) and recorded as a function of temperature. The amount of available surface atoms of Cu and Pd nanoparticle in the series of Cu-Pd/U₅₀S₅₀ was determined by a pulse chemisorption

method; CO chemisorption for the Pd active sites and N₂O chemisorption for Cu active sites. The pulse chemisorption experiments were performed using a dynamic flow method at 50 °C on a BELCAT-M equipped with a W-Re filament TCD. Each catalyst sample was placed into a quartz sample cell and then pretreated with the following procedure before the chemisorption measurement: (i) sample was initially purged and heated to 250 °C (for CO chemisorption) or 350 °C (for N₂O chemisorption) under He (99.999%) with a 10 °C min^{−1} ramping rate, (ii) sample was reduced at the same temperature under H₂ (99.999%) for 60 min, (iii) sample was finally purged and cooled to 50 °C under He (99.999%) for about 45 min and held for 15 min. The pulse CO measurement was conducted by charging the 0.988 uL gas loop volume with 5% CO/He for 5 min and then injecting into the sample. The charging and injection steps were repeated until the peak area detection from the TCD signal reach an equilibrium state and the adsorbed CO gas volume was obtained to calculate the metal dispersion. Similarly, 5% N₂O/Ar was used to determine the available Cu surface atoms by dissociative nitrous oxide chemisorption as follows.



The result of metal dispersion, metal surface area, and turn over frequencies (TOFs) based on CO- and N₂O-chemisorption for Pd and Cu metal active sites, respectively, were listed in Table S3.

2.5. Products analysis

The reaction products were qualitatively analyzed using gas chromatography–time of flight mass spectrometry (GC-TOF/MS). An Agilent 7890N GC (Agilent Technologies, USA) and Pegasus high-throughput (HT) TOF-MS system (Leco Corporation, USA) were equipped with an auto injector (Agilent 7860N) and middle-range polarity, Rxi-5Sil-MS, column (30 m × 0.25 μm × 0.25 mm ID). Ultrahigh purity helium (99.9999%) was used as a carrier gas at a 1.0 mL min^{−1} flow rate. Typically, 1 μL of the products recovered right after the reaction was injected into the column in a split mode of 25:1. The injector temperature was set at 250 °C, while the transfer line temperature was fixed at 260 °C. The column temperature was programmed to initiate heating starting from 40 °C, held for 2 min, and then increased to 300 °C with a 10 °C min^{−1} heating rate. The detectable mass range for the MS was set at 35–650 m/z. A GC equipped with a flame ionization detector (FID) was used to quantify the reaction products. An Agilent 6890N GC was equipped with a 30 m × 0.25 μm × 0.25 mm inner diameter Rxi-5Sil-MS capillary column. One microliter of the liquid product recovered right after the reaction was injected into the GC with a split ratio 1:10. The inlet and detector temperatures were fixed at 250 °C. The initial column temperature was 40 °C (2 min) with a 10 °C min^{−1} heating rate. The final temperature was 250 °C. All product yields and selectivities were calculated by an external standard calibration curve.

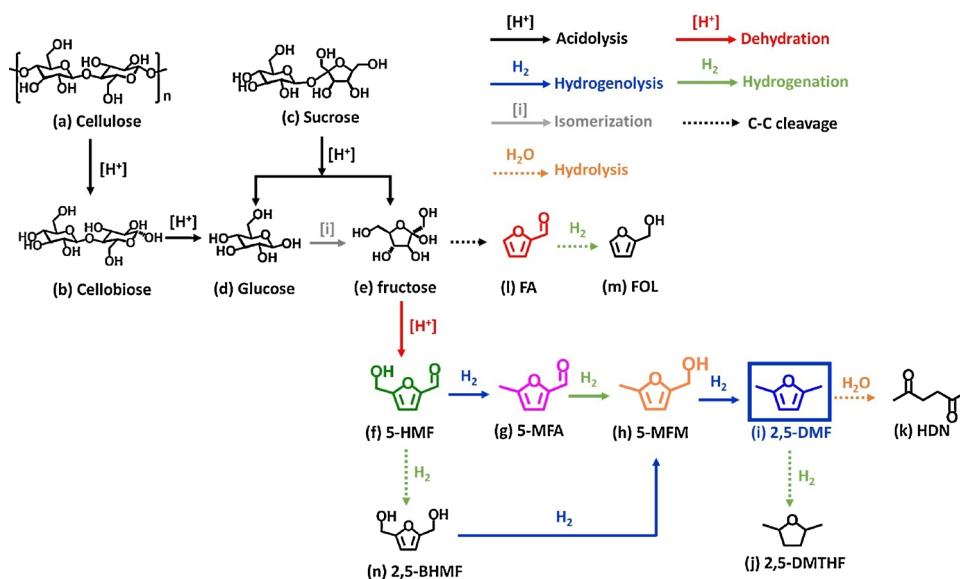
The conversions of monosaccharides, disaccharides, and polysaccharides were calculated using Eq. (1) assuming the *in situ* formed water is utilized to initiate acid-hydrolysis (step 1) mediating the proton transfer (H₃O⁺) and to stabilize intermediate species [26] and negligible amount of saccharides are soluble in the THF-rich condition by the produced water.

$$\text{Conversion}(\%) = \frac{\text{Weight of initial reactant} - \text{weight of solid residue}}{\text{weight of initial reactant}} \times 100\% \quad (1)$$

The yield and selectivity of 2,5-DMF from three different types of reactants, including monosaccharide (fructose and glucose), disaccharide (sucrose and cellobiose), and polysaccharide (starch and cellulose), were calculated using Eqs. (2)–(7).

If monosaccharides (glucose and fructose) were used as reactants:

$$2, 5 - \text{DMF yield}(\text{mol}\%) = \frac{\text{mol of 2, 5-DMF}}{\text{mol of monosaccharide feed}} \times 100\% \quad (2)$$



Scheme 2. Plausible reaction pathway for di- and polysaccharide conversion into 2,5-dimethylfuran. (a) cellulose, (b) cellobiose, (c) sucrose, (d) glucose, (e) fructose, (f) 5-hydroxymethylfurfural (5-HMF), (g) 5-methylfurfural (5-MFA), (h) 5-methyl-2-furanmethanol (5-MFM), (i) 2,5-dimethylfuran (2,5-DMF), (j) 2,5-dimethyltetrahydrofuran (2,5-DMTHF), (k) 2,5-hexanedione (HDN), (l) furfural (FA), (m) furfuryl alcohol (FOL), and (n) 2,5-bis-hydroxymethylfurfural (2,5-BHMF).

$$2.5 - \text{DMF selectivity}(\text{mol}\%) = \frac{\text{mol of 2, 5-DMF}}{\text{mol of reacted monosaccharide}} \times 100\% \quad (3)$$

If disaccharides (cellobiose and sucrose) used as reactant:

$$2.5 - \text{DMF yield}(\text{mol}\%) = \frac{\text{mol of 2, 5-DMF}}{2 \times \text{mol of disaccharide feed}} \times 100\% \quad (4)$$

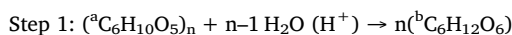
$$2.5 - \text{DMF selectivity}(\text{mol}\%) = \frac{\text{mol of 2, 5-DMF}}{2 \times \text{mol reacted disaccharide}} \times 100\% \quad (5)$$

If polysaccharides (starch and cellulose) were used as reactants:

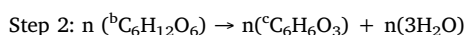
$$2.5 - \text{DMF yield}(\text{mol}\%) = \frac{\text{mol of 2, 5-DMF}}{\text{mol of } \text{C}_6\text{H}_{10}\text{O}_5 \text{ unit in the initial feed}} \times 100\% \quad (6)$$

$$2.5 - \text{DMF selectivity}(\text{mol}\%) = \frac{\text{mol of 2, 5-DMF}}{\text{mol of reacted } \text{C}_6\text{H}_{10}\text{O}_5 \text{ unit}} \times 100\% \quad (7)$$

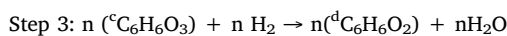
The step reaction for polysaccharide conversion to 2,5-DMF through acid-hydrolysis, hydrogenation, and hydrogenolysis is shown below,



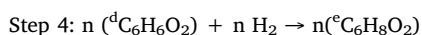
(hydrolysis/acidolysis of ^acellulose to ^bglucose)



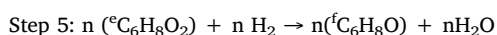
(dehydration of ^bfructose to ^c5-HMF)



(hydrogenolysis of ^c5-HMF to ^d5-MFA)



(hydrogenation of ^d5-MFA to ^e5-MFM)



(hydrogenolysis of ^e5-MFM to 2,5-DMF) where 5-HMF is 5-hydroxymethylfurfural, 5-MFA is 5-methylfurfural, 5-MFM is 5-methyl-2-furanmethanol, and 2,5-DMF is 2,5-dimethylfuran. The reaction scheme of cellulose and sucrose conversion into 2,5-DMF is shown in Scheme 2.

2.6. Density functional theory (DFT) calculations

Density functional theory (DFT) calculations were carried out to determine the most stable structure of an isolated UiO-66 and UiO-66(NH₂) node using the DMol³ program [27]. The generalized gradient approximation with the Perdew–Burke–Ernzerhof functional [28] was employed to describe the exchange-correlation energy of electrons. Double numerical basis sets with polarization functions under a 3.5 level were used. The semi-empirical dispersion correction method proposed by Tkatchenko and Scheffler [29] was applied to correct the simulated structure by considering the van der Waals dispersion effects. The convergence criteria for the geometry optimization were set with an energy tolerance of 1.0×10^{-5} Ha, a maximum force tolerance of $0.002 \text{ Ha } \text{\AA}^{-1}$, and a maximum displacement of 0.005 \AA . The binding energy was calculated as the difference of energy between the product and reactants in the adsorption process, as defined in Eq. (8).

$$\text{Binding energy} = E_{\text{MOF-5-HMF}} - E_{\text{MOF}} - E_{5\text{-HMF}} \quad (8)$$

where $E_{\text{MOF-5-HMF}}$ is the total energy of the MOF-5-HMF system at equilibrium and E_{MOF} and $E_{5\text{-HMF}}$ is the energy of the 5-HMF-free MOF and the singular 5-HMF, respectively.

3. Result and discussion

3.1. Catalyst characterization

Figs. 1a and S1(a) show XRD patterns of the UiO-66(NH₂) and the catalysts with various Cu and Pd loadings on UiO-66(NH₂)@SGO with a UiO-66(NH₂):SGO weight ratio of 50:50 (which is denoted as U₅₀S₅₀). The experimental metal loadings, determined using ICP-OES, are listed in Table 1. As shown in Fig. 1, the crystalline phases of the as-synthesized UiO-66(NH₂) were well-matched with those of the simulated UiO-66(NH₂) using Rietveld refinement (conducted by Materials studio, Accelrys Software Inc.), indicating that the as-synthesized material exhibited the crystal structure of UiO-66(NH₂). The as-synthesized UiO-66(NH₂) exhibited broad peaks with low intensity, suggesting that some degree of amorphosity existed. This was caused by missing some of the organic linkers (2-aminoterephthalate, C₆H₃NH₂(CO₂)₂) during the HCl-modulated synthesis [12,22], as will be discussed in a later section. As shown in Fig. 1a, the XRD pattern of the 2 wt% Pd-loaded catalyst (2Pd/U₅₀S₅₀) was very similar to that of UiO-66(NH₂), indicating that a low amount of Pd loading did not cause a significant change in the crystalline structure of the support. A closer inspection of the XRD patterns shown in Fig. 1b revealed that the (111) plane of Pd at

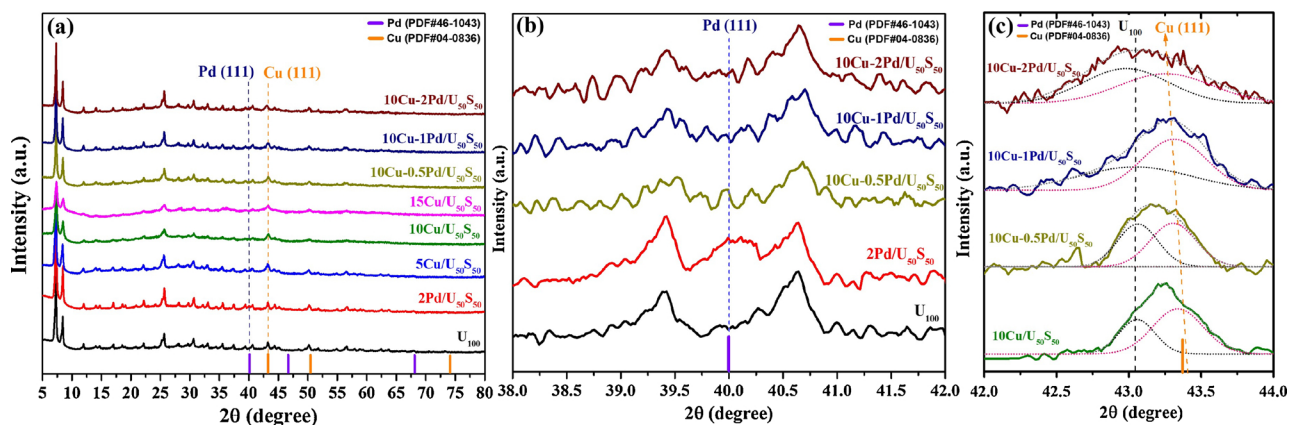


Fig. 1. (a) XRD patterns of UiO-66(NH₂) and Cu-Pd/UiO-66(NH₂)/SGO catalysts with various Cu and Pd loadings along with JCPDS database of Cu (JCPDS file #04-0836) and Pd (JCPDS file #46-1043), (b) enlarged area of the XRD patterns at 2θ ranging from 38° to 42°, and (c) enlarged area of the 10Cu-Pd/U₅₀S₅₀ XRD patterns for 2θ ranging from 42° to 44° at various Pd loading values and the corresponding deconvolution peaks of Cu (pink dotted-line) and UiO-66(NH₂) (black-dotted line). The weight ratio of UiO-66(NH₂):SGO in U₅₀S₅₀ was 50:50.

2θ = 40.1° was present in the 2Pd/U₅₀S₅₀ catalyst, which matches with the metallic Pd (JCPDS file #46-1043). On the other hand, the crystallinity of the UiO-66(NH₂) sample decreased after Cu loading; the intensity of the main peaks of UiO-66(NH₂) at 2θ = 7.3° and 8.5° decreased gradually as Cu loadings increased from 5 to 15 wt%. Because the Cu (111) plane at 2θ = 43.5° (JCPDS file #04-0836) overlapped with one of the UiO-66(NH₂) peaks near 2θ = 43°–44°, in-depth analysis of the XRD patterns was carried out, and the results are shown in Fig. 1c. The peak at 2θ = 43°–44° was deconvoluted using the UiO-66(NH₂) peaks at 43.1° (which was determined using the simulation, Fig. S1a) and of the Cu (111) plane at 2θ = 43.5°. The peak deconvolution results revealed that the Cu peak position shifted slightly towards lower angles (from 43.42° to 43.39°) as Pd loading increased from 0 to 2 wt%. This Cu peak shifting implies that the simultaneous Pd and Cu loading affected the crystalline structure of Cu, which could be caused by the formation of a Cu-Pd alloy with a low alloying degree [30–32].

To investigate the degree of organic linker missed in the UiO-66(NH₂) structure, the thermal decomposition behavior was examined using TGA and differential thermal analysis (DTA), as shown in Fig. 2. The TGA profile at temperatures ranging from 275 to 700 °C can be attributed to the transformation of Zr₆O₆(C₈H₅NO₄)₆ into ZrO₂ by the

decomposition of organic 2-aminoterephthalate (C₆H₃NH₂(CO₂)₂) in the UiO-66(NH₂) framework [22,33]. The mass-loss below 275 °C (represented by regions (i) and (ii) in Fig. 2) could be caused by the evaporation of moisture/entrapped solvent and the removal of co-ordinated hydroxyl group at Zr voids through dehydration, respectively. The thermal decomposition in region (iii) at 275–700 °C exhibited a lower weight loss of 45 wt% (from 83 wt% to 38 wt%) than the theoretically calculated weight loss for a perfect UiO-66(NH₂) crystal (57 wt%), which is estimated based on the assumption that a total of six C₆H₃NH₂(CO₂)₂ linkers per unit formula of Zr₆O₆(C₈H₅NO₄)₆ are located in the framework). This result indicates that the structure vacancies in the as-synthesized UiO-66(NH₂) existed, which is caused by the missed C₆H₃NH₂(CO₂)₂ linkers in the framework. To quantify the amount of C₆H₃NH₂(CO₂)₂ linkers missed in the as-synthesized UiO-66(NH₂), the approach through thermal decomposition method was employed. As shown in Fig. S2 and described in the Supplementary data, the number of organic-linkers is approximately 4 per unit formula of Zr₆O₆(C₈H₅NO₄)_x, indicating that the as-synthesized UiO-66(NH₂) having around 33.8% linker vacancies.

Along with these crystallinity changes in the US support, the metal loading on the support has an influence on the textural properties of the

Table 1

Physicochemical and textural properties of UiO-66(NH₂), UiO-66(NH₂)/SGO, and Cu-Pd/UiO-66(NH₂)/SGO catalysts with various Cu and Pd loading values.

| Catalysts | Metal loading on the US support | | | N ₂ adsorption-desorption isotherm analysis ^c | | |
|--|---------------------------------|---|---|---|--------------------|---|
| | Theoretical metal loading (wt%) | Experimental metal loading ^a (wt%) | Cu ⁰ /Cu ²⁺ 2p ^{3/2} atomic surface composition ^b (%) | | | |
| | Cu/Pd | Cu/Pd | Cu ⁰ /Cu ²⁺ | specific surface area (m ² g ⁻¹) | Pore diameter (nm) | Pore volume ^d (cm ³ g ⁻¹) |
| UiO-66(NH ₂) | – | – | – | 1202.9 | 0.7 | 0.68 |
| UiO-66(NH ₂)/SGO (U ₅₀ S ₅₀) ^e | – | – | – | 665.7 | 0.7 | 0.37 |
| 10Cu/U ₅₀ S ₅₀ | 10/0 | 8.96/0 | 45.6/54.4 | 415.2 | 0.7 | 0.34 |
| 15Cu/U ₅₀ S ₅₀ | 15/0 | N.M. ^f | N.M. ^f | 239.8 | 0.7 | 0.12 |
| 2Pd/U ₅₀ S ₅₀ | 0/2 | 0/2.04 | – | 489.5 | 0.7 | 0.34 |
| 10Cu-0.5Pd/U ₅₀ S ₅₀ | 10/0.5 | 9.32/0.41 | 47.3/52.7 | 312.2 | 0.7 | 0.25 |
| 10Cu-1Pd/U ₅₀ S ₅₀ | 10/1 | 9.09/0.89 | 51.2/48.8 | 307.4 | 0.7 | 0.25 |
| 10Cu-2Pd/U ₅₀ S ₅₀ | 10/2 | 10.02/1.91 | 42.7/57.3 | 304.8 | 0.7 | 0.25 |
| 10Cu-1Pd/U ₅₀ S ₅₀ (spent) | – | 9.0/0.75 | 51.2/48.8 | 282.3 | 0.7 | 0.24 |

^a The experimental metal loadings in the catalysts were determined using ICP-OES.

^b The atomic surface composition of Cu⁰ 2p^{3/2} (B.E: 932 eV) and Cu²⁺ 2p^{3/2} (B.E: 934 eV) were determined using XPS.

^c N₂ adsorption-desorption analysis was measured using the BET method.

^d Total pore volume was measured at p/p₀ = 0.989.

^e Weight ratio of UiO-66(NH₂):SGO was 50:50.

^f N.M.: not measured.

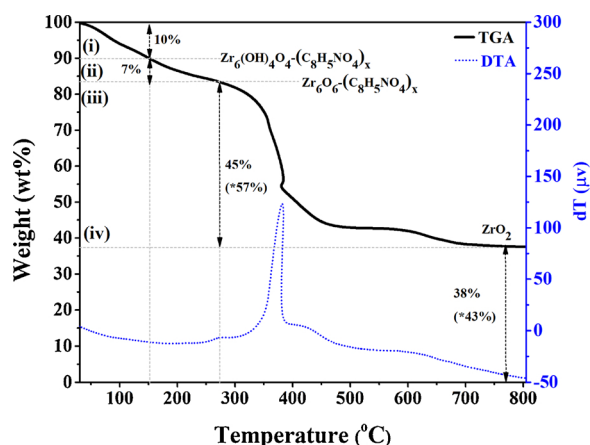


Fig. 2. TGA and DTA profiles of UiO-66(NH₂) in air. The weight decomposition area was divided into four major regions of (i) evaporation of volatile species at 30–150 °C, (ii) dehydration of hydroxylated UiO-66(NH₂) (Zr₆(OH₄)O₄-(C₈H₅NO₄)_x) at 150–275 °C, (iii) decomposition of dehydroxylated UiO-66(NH₂) (Zr₆O₆-(C₈H₅NO₄)_x) at 275–600 °C, and (iv) the remaining ZrO₂ at 600–800 °C. The presented weight percent values at the corresponding dotted arrows represented the weight loss, and the number in parentheses represents the weight loss caused by the theoretical decomposition of Zr₆O₆-(C₈H₅NO₄)₆ into ZrO₂.

catalysts, as shown in Fig. 3a and listed in Table 1. The N₂ adsorption-desorption isotherms of the U₅₀S₅₀ support and the Cu-Pd/U₅₀S₅₀ catalysts followed the type-I pattern, indicating the presence of micropores. The pore size distribution of the micropore region, analyzed using the MP plot method, show that most of pores had sizes ranging from 0.6 nm to 1.2 nm with an average pore diameter of ~0.7 nm. The lower BET surface area of U₅₀S₅₀ (665.7 m² g⁻¹) compared to that of the as-synthesized UiO-66(NH₂) (1202.9 m² g⁻¹) is caused by the inherent low surface area of SGO. As the Cu loading increased to 15 wt%, the BET surface area decreased significantly to 239.8 m² g⁻¹ and pore volume decreased to 0.12 cm³ g⁻¹. This indicates that some fraction of the porous host-framework structure of UiO-66(NH₂) was occupying the metal phase.

The surface composition and elemental chemical states of the catalyst were investigated using XPS. The wide-scan spectrum and the high-resolution spectra of the individual elements, which are shown in Fig. S3, indicate the presence of Cu, Pd, Zr, O, N, C, and S in 10Cu-1Pd/U₅₀S₅₀. To further investigate possible changes in the elemental chemical states of Pd and Cu in the bimetallic Cu-Pd/U₅₀S₅₀ catalysts, the Pd 3d_{5/2} and Cu 2p_{3/2} regions of monometallic 1Pd/U₅₀S₅₀ (Fig. 4a) and 10Cu/U₅₀S₅₀ (Fig. 4d) catalysts were compared with those of bimetallic 10Cu-1Pd/U₅₀S₅₀ (Fig. 4b and e) and 10Cu-2Pd/U₅₀S₅₀ (Fig. 4c and f) catalysts. The Pd peaks at 335.5 eV and 341.3 eV correspond to metallic Pd⁰ 3d_{5/2} and Pd⁰ 3d_{3/2}, respectively [12]. The Pd 3d_{5/2} peak at 335.5 eV in 1Pd/U₅₀S₅₀ was slightly shifted towards the low-binding-energy direction (335.3 eV) in the bimetallic 10Cu-1Pd/U₅₀S₅₀ and 10Cu-2Pd/U₅₀S₅₀ catalysts. In addition, the incorporation of 2 wt% Pd resulted in the Cu⁰ 2p_{3/2} peak shifting to the low-binding-energy direction from 932.1 eV (10Cu/U₅₀S₅₀) to 931.9 eV (10Cu-2Pd/U₅₀S₅₀). The peak shifting to the low-binding-energy direction of the bimetallic Cu-Pd catalysts suggests that interatomic electron transfer occur between Cu and Pd [34], which results from the electronegativity difference between Cu and Pd metals. This allows the electrons to flow from Cu (χ = 1.9) to Pd (χ = 2.2) [35], which could be caused by an adjustment of the d-band center position (or hybridization) [36]. The observed-peak shifting towards the low-binding-energy direction as the Pd content increased from 0 to 2 wt% was possibly caused by crystal lattice strain in the Cu and Pd phase rearrangement as the corresponding metals formed an alloy [36], which agree well with the XRD pattern of Cu (111).

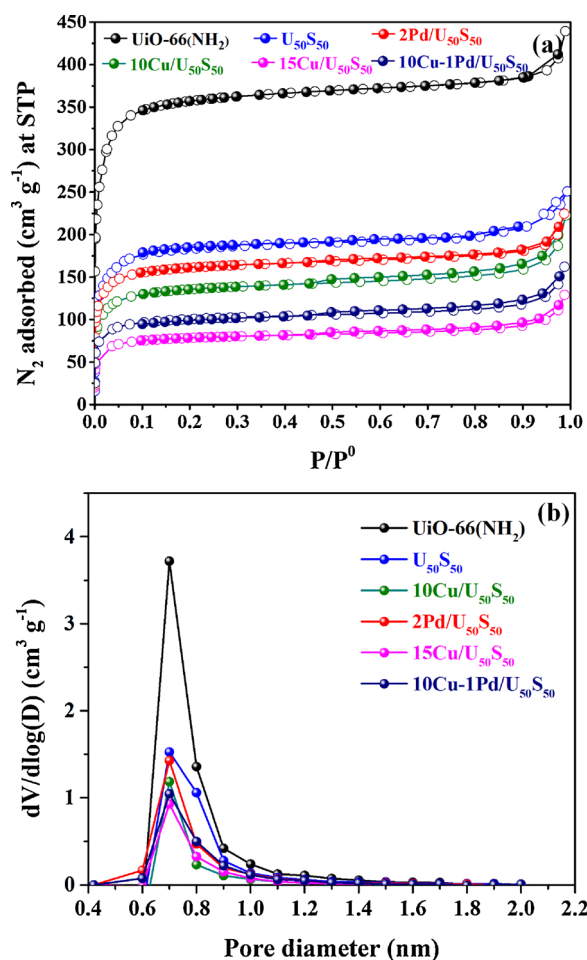


Fig. 3. (a) N₂ adsorption-desorption isotherms and (b) distribution of micropores measured by the MP method of the U₅₀S₅₀ support and the Cu-Pd/U₅₀S₅₀ catalysts with various Cu and Pd loading values.

In this work, we hypothesized that the hydrogenolysis and hydrogenation activity to produce 2,5-DMF were closely related to the active metallic phase of Cu-, Pd-, and Cu-Pd. Hence, the ability of Cu, Pd, and Cu-Pd to facilitate the hydrogenation and hydrogenolysis reactions were further investigated by hydrogen uptake experiments. The H₂-TPR technique was employed to characterize the surface and bulk oxygen reducibility of the catalysts, and the results are shown in Fig. 5. The H₂-TPR profiles of the catalysts exhibited the hydrogen uptake in two different regions; the peaks at temperatures below 350 °C were contributed by the metal species, whereas the peaks at temperatures above 350 °C were contributed by the characteristics of the support material. The U₅₀S₅₀ support did not show any specific reduction peak in the H₂-TPR profile below 300 °C, which confirms the absence of reducible species in the support. The very broad hump at after 350 °C can be caused by the reduction of the surface oxygenated species of SGO. High reduction temperatures (> 500 °C) was required to reduce the surface acidic groups on the SGO surface, as previously shown in the TPR profile for activated carbon [37]. Additionally, in correlation with the thermal decomposition behavior (Fig. 2), the peak centered at 550 °C can be possibly corresponding to the structural degradation occurred due to inherent thermal instability of UiO-66(NH₂) at temperatures higher than 350 °C.

After Cu and Pd loading, some noticeable reduction peaks started to appear at temperatures below the decomposition temperature of the U₅₀S₅₀ support. The monometallic 2Pd/U₅₀S₅₀ catalyst shows a single broad peak centered at 193 °C, which is attributed to the reduction of PdO phases [38]. The PdO phases is present on the surface of Pd

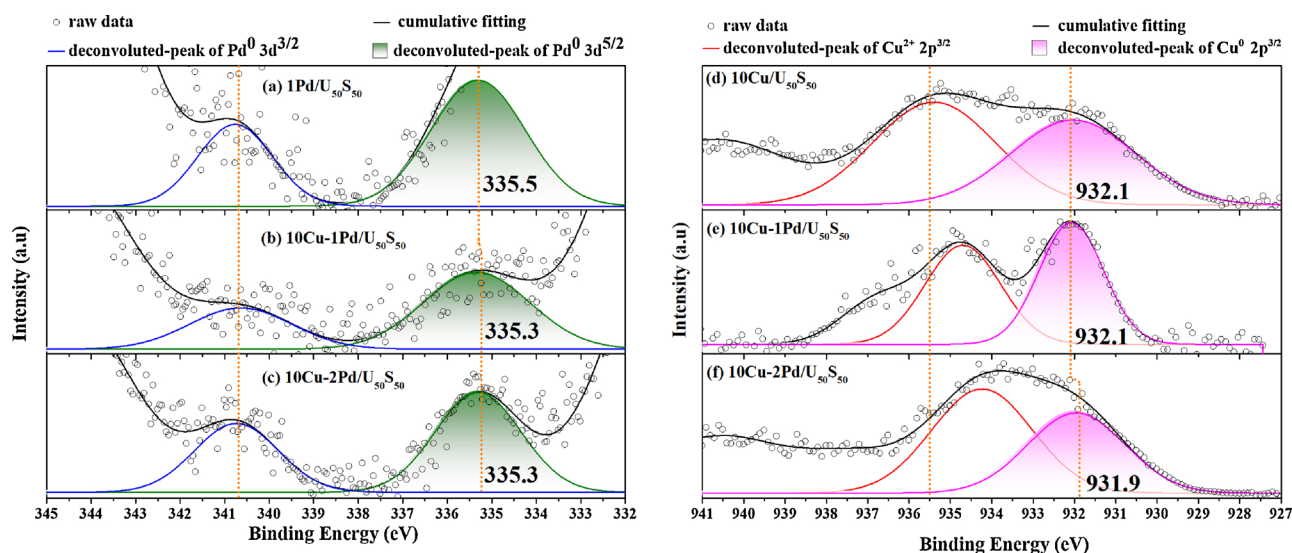


Fig. 4. Deconvoluted XPS core-level spectra of Pd 3d and Cu 2p^{3/2} states of the Cu-Pd/U₅₀S₅₀ catalysts with various Cu and Pd loading values. The numbers in the graph represent the binding energy at maximum intensity of the corresponding metallic states.

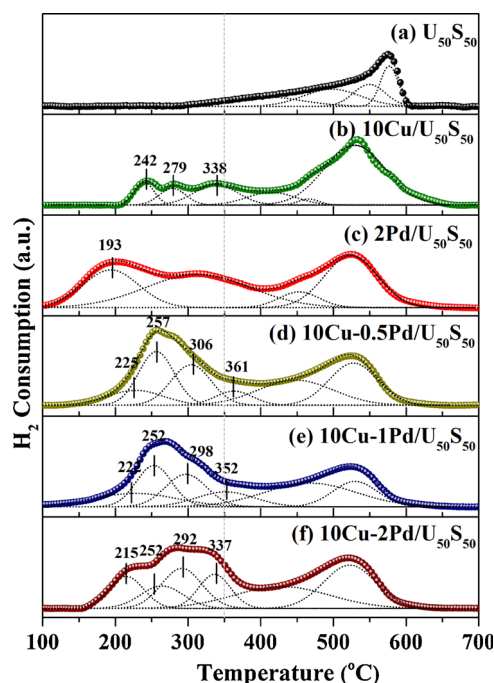


Fig. 5. H₂-TPR profiles of the U₅₀S₅₀ support and the Cu-Pd/U₅₀S₅₀ catalysts with various Cu and Pd loading values. The dotted lines under the profile represent the deconvolution peaks. The dotted grey lines area represented the maximum H₂-uptake temperature prior to the decomposition of the US support at 350 °C.

nanoparticles, which can be re-oxidized after making contact with air [39]. On the other hand, the monometallic 10Cu/U₅₀S₅₀ catalyst exhibited multiple H₂ consumption peaks at temperatures between 200 and 350 °C, which can be associated with the consecutive reduction of Cu²⁺ to Cu⁺ and Cu⁰ [40]. The initial two peaks at 242 and 279 °C can be assigned to the reduction of isolated Cu²⁺ ions and CuO present in the cavity, respectively [40]. The high-temperature reduction at 338 °C can be attributed to the reduction of Cu⁺ to Cu⁰. All the bimetallic Cu-Pd/U₅₀S₅₀ catalysts exhibited at least four peaks centered at 217–231 °C, 253–257 °C, 283–291 °C and 324–350 °C. As compared to monometallic 10Cu/U₅₀S₅₀, the peaks in the bimetallic Cu-Pd/U₅₀S₅₀ catalysts shifted towards lower reduction temperatures, which reveals

that the synergistic interaction between Cu and Pd enhanced the reducibility of the Cu species. As detected in the metal-free U₅₀S₅₀ support, bimetallic Cu-Pd/U₅₀S₅₀ exhibited broad hump peak after 350 °C centered at around 550 °C due to the characteristics of the U₅₀S₅₀ support.

The morphology of the bimetallic 10Cu-1Pd/U₅₀S₅₀ catalyst was investigated by SEM-EDX along with elemental mapping. The size of Cu and Pd were analyzed using HR-TEM. A uniform distribution of C, N, Zr, Cu, Pd, and S on the 10Cu-1Pd/U₅₀S₅₀ catalyst was observed in Fig. S4. The low-magnification HR-TEM image (Fig. 6a) shows that nano-sized Pd and Cu are uniformly deposited on the surface of UiO-66(NH₂). The size distribution of Pd and Cu were in the range of 2–9 nm with an average size of 5.1 nm (inset of Fig. 6b). The metal-loaded UiO-66(NH₂) particles were incorporated into the SGO sheets. The high-magnification HR-TEM image shown in Fig. 6b indicates that *d*_{TEM}-spacings existed in the metal phase. The 0.240 nm and 0.213 nm peaks were matched with JCPDS file #07-0138, which belongs to the Cu₃Pd structure. The XRD patterns related to the corresponding *d*_{TEM}-spacing of 0.240 nm ($2\theta = 36.4^\circ$) and 0.213 nm ($2\theta = 42.3^\circ$) were not observed in the 10Cu-1Pd/U₅₀S₅₀ catalyst, which can be caused by low abundance of the Cu₃Pd phase below the detection limit of XRD. Fig. 6c shows that a Cu-Pd alloy formed at the interfaces between Cu and Pd nanoparticles, and thus the overall amount of the Cu-Pd alloy phase is much smaller compared to isolated Cu and Pd phases. In some portions of the 10Cu-1Pd/U₅₀S₅₀ catalyst, discrete Pd (Fig. 6d) and Cu particles (Fig. 6e) were observed. An in-depth analysis of the Cu-Pd alloy was further carried out by performing EDS mapping analysis using STEM and HAADF. As presented in Fig. 6f, by depicting the illumination contrast of the obtained image in Fig. 6f(i), brighter sphere-like spots are representative of the metal phases, suggesting the Cu-Pd nanoparticles are well-dispersed on the U₅₀S₅₀ support. As shown in Fig. 6f(ii)–(iv), in particular areas of the catalyst (which are indicated by white square boxes in the Fig.), the cluster islands containing both Cu (yellow) and Pd (green) were located at the edge of the UiO-66(NH₂) phase boundaries. Therefore, as evidenced by Fig. 6b–c and f, in some area of the Cu-Pd bimetallic catalyst, a close contact between Pd and Cu phases led to the formation of a Pd-Cu alloying phase at the interface between the individual Cu and Pd phases during heat-treatment. The acidic sites in UiO-66(NH₂), SGO, and the US supports with various weight ratios UiO-66(NH₂) and SGO were evaluated by Py-FTIR spectroscopy and acid-base neutralization. The results are shown in Fig. 7. The presence of Brønsted and Lewis acid sites in the supports were

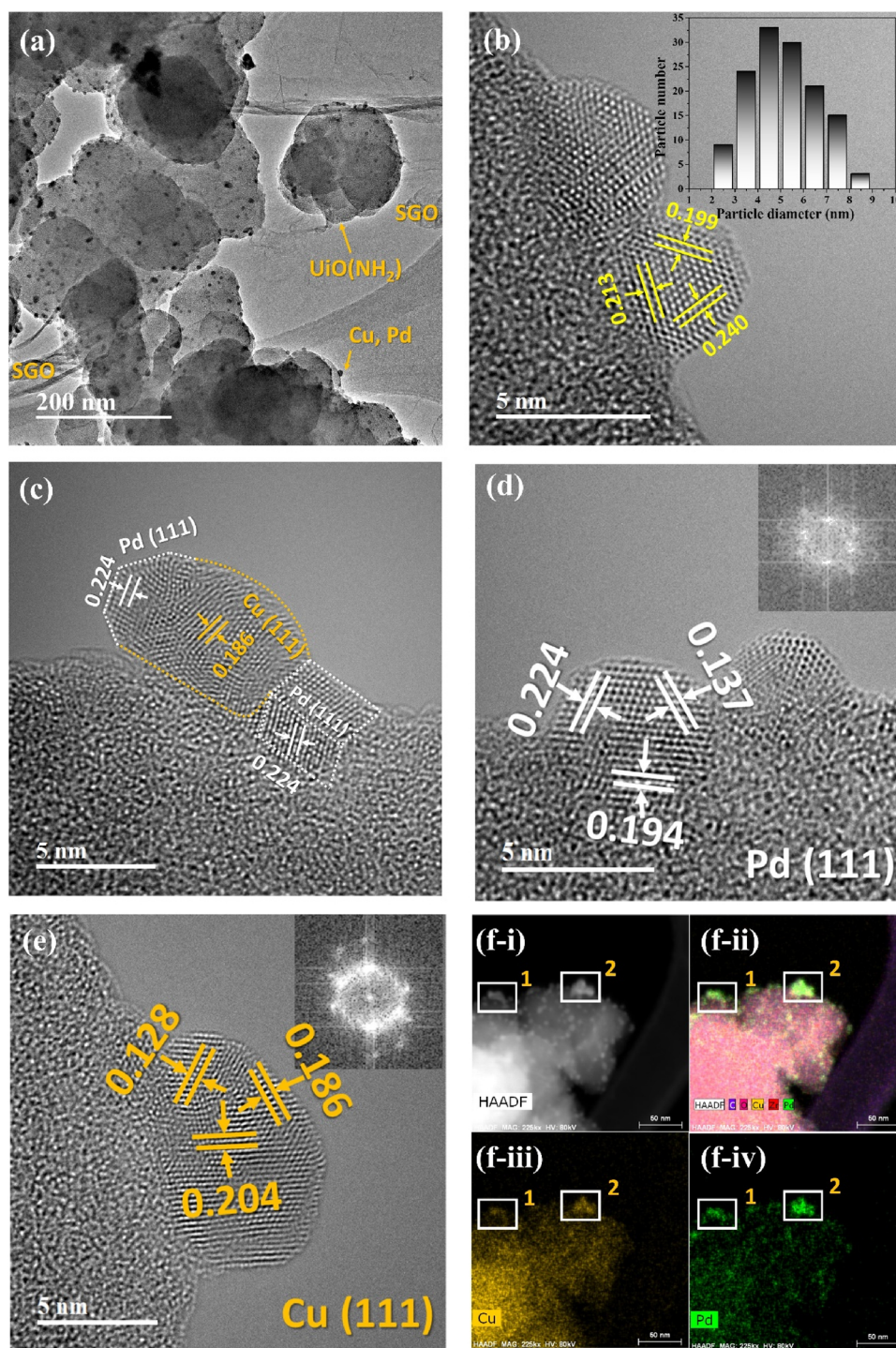


Fig. 6. (a)–(e) HR-TEM images and (f) HAADF-STEM image with EDS elemental map of 10Cu-1Pd/U₅₀S₅₀. Inset in Fig. 6b: particle size distribution of Cu-Pd in 10Cu-1Pd/U₅₀S₅₀. Inset in Fig. 6d: the inverse FFT for the interplanar spacing of the Pd (111). Inset in Fig. 6e: the inverse FFT for the interplanar spacing of the Cu (111).

evidenced by probing the support with pyridine adsorption bands at IR frequencies ranging from 1600 to 1400 cm^{-1} . These bands are related to vibrational modes of the ring breathing $\nu(\text{C}=\text{N})$ originating from the interaction between pyridine and the acid sites of the catalyst [41]. The adsorbed-pyridine spectra were evaluated based on two main regions of 1535 cm^{-1} and 1446 cm^{-1} , which are attributed to the Brønsted and Lewis acid sites, respectively. The broad and multiple peaks in the 1500–1600 cm^{-1} frequency range in the US supports are caused by overlapping IR absorption bands generated from the carboxylate groups (COO^-) and phenyl ($\text{C}=\text{C}$) units [42], which are different from the

relatively sharp pyridine-IR bands of metal oxide catalysts. Therefore, careful inspection of the obtained-IR bands from adsorbed pyridine spectra was attempted by deconvoluting the peaks of 1500–1600 cm^{-1} frequency range after evaluating the non-pyridine probed FTIR spectra of UiO-66(NH_2) and SGO (see Fig. S5). The rigorous deconvolution of the FTIR spectra has been proposed in previously reported studies on MOF-based materials [43] using the Pearson-VII curve fitting method due to its flexibility towards IR-spectra patterns utilizing Gaussian and Lorentzian functions. Using the curve-fitting method, Brønsted acidic peak contributed from the pyridine interaction with Zr-OH species of

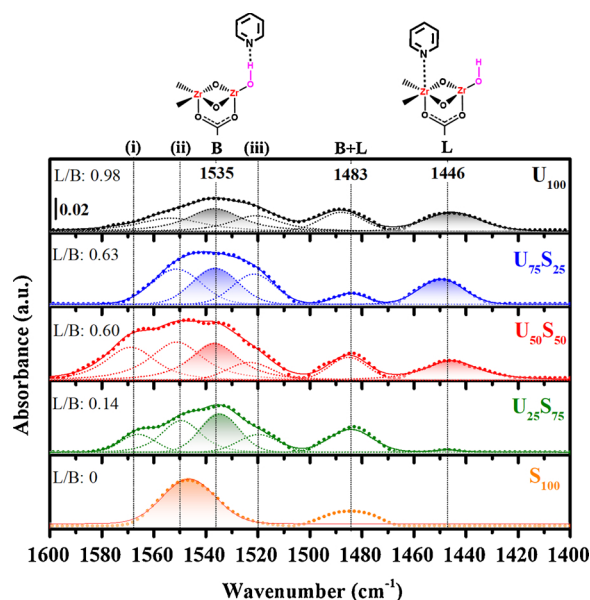


Fig. 7. Pyridine-probed FT-IR spectra with specific molecular vibration band of asymmetric O–C=O at (i) 1569 cm^{-1} , (ii) 1550 cm^{-1} and (iii) 1520 cm^{-1} . Brønsted acid site from pyridine-Zr-OH interaction at 1535 cm^{-1} (B), and Lewis acid site from pyridine-Zr⁴⁺ interaction at 1446 cm^{-1} (L). Acidity characterization of the UiO-66(NH₂) (U₁₀₀), SGO (S₁₀₀), and the US supports of U₂₅S₇₅ (UiO-66(NH₂): SGO = 25:75); U₅₀S₅₀ (UiO-66(NH₂): SGO = 50:50); and U₇₅S₂₅ (UiO-66(NH₂): SGO = 75:25).

Table 2

Acidity properties of the SGO, UiO-66(NH₂)@SGO with various UiO-66(NH₂):SGO ratios, and Cu-Pd/UiO-66(NH₂)@SGO with various Cu and Pd loadings.

| Catalyst | Proton concentration ^a ([H ⁺], mmol g ⁻¹) | Brønsted acid sites ^b (B, mmol g ⁻¹) | Lewis acid sites ^c (L, mmol g ⁻¹) | L/B ratio |
|--|---|---|--|-----------|
| ^d S ₁₀₀ | 2.48 | 0.85 | N.D. ⁱ | 0 |
| ^e U ₂₅ S ₇₅ | 2.39 | 0.64 | 0.09 | 0.14 |
| ^f U ₅₀ S ₅₀ | 2.55 | 1.02 | 0.61 | 0.60 |
| ^g U ₇₅ S ₂₅ | 2.69 | 0.82 | 0.52 | 0.63 |
| ^h U ₁₀₀ | 2.03 | 0.52 | 0.51 | 0.98 |
| 5Cu/U ₅₀ S ₅₀ | 2.50 | – | – | – |
| 10Cu/U ₅₀ S ₅₀ | 2.21 | – | – | – |
| 15Cu/U ₅₀ S ₅₀ | 2.38 | – | – | – |
| 2Pd/U ₅₀ S ₅₀ | 2.45 | – | – | – |
| 10Cu-0.5Pd/ U ₅₀ S ₅₀ | 2.19 | – | – | – |
| 10Cu-1Pd/ U ₅₀ S ₅₀ | 2.11 | – | – | – |
| 10Cu-2Pd/ U ₅₀ S ₅₀ | 2.08 | – | – | – |

^a The proton concentrations ([H⁺]) were measured by acid-base neutralization via potentiometric titration with 0.0114 M standardized-NaOH as a titrant.

^b Brønsted acid sites (B) were determined using pyridine-probed FT-IR at 1535 cm^{-1} .

^c Lewis acid (L) sites were determined by pyridine-probed FT-IR at 1446 cm^{-1} .

^d 100% SGO support.

^e SGO: UiO-66(NH₂) = 25:75.

^f SGO: UiO-66(NH₂) = 50:50.

^g SGO: UiO-66(NH₂) = 75:25.

^h 100% UiO-66(NH₂) support.

ⁱ Not detected in pyridine-probed FT-IR.

UiO-66(NH₂) at 1535 cm^{-1} was well-defined apart from the carboxylate group vibrations of (i) and (ii) at 1569 cm^{-1} [33] and 1550 cm^{-1} [44], respectively. The calculated Brønsted and Lewis acid strength and the ratio of Lewis-to-Brønsted acidity (L/B ratio) were listed in Table 2.

As the UiO-66(NH₂) content increased in the US supports, the L/B ratio increased from 0.14 (U₂₅S₇₅) to 0.63 (U₇₅S₂₅). The enriched Lewis acid sites originating from unsaturated Zr⁴⁺ cores in UiO-66(NH₂) at 1446 cm^{-1} is responsible for the increase in L/B ratio with increasing UiO-66(NH₂) content. To quantify the Brønsted acid site, the US supports with different UiO-66(NH₂):SGO ratios were characterized using the acid-base potentiometric neutralization method. As shown in Fig. S6, the amount of titrant required for neutralization increased with increasing UiO-66(NH₂) content. Proton concentration ([H⁺]) was calculated based on the titration curves, and the results are listed in Table 2. As the UiO-66(NH₂) content increased, the Proton concentration ([H⁺]) increased from 2.39 to 2.69 mmol g⁻¹. By controlling the relative amount of UiO-66(NH₂) and SGO in the US support, the Lewis and Brønsted acid ratio in the catalyst can be adjusted. This ratio plays an important role in mediating sequential glycosidic-bond cleavage through acidolysis, isomerization, and dehydration, as will be discussed in the following sections.

3.2. Evaluation of catalytic activity

3.2.1. Screening of the UiO-66(NH₂)@SGO (US) supports

Previously, the role of a solvent in initially directing the conversion of monosaccharides (glucose and fructose) to 5-HMF through the dehydration reaction was reported in our and other previous papers [12,45,46]. We previously demonstrated that THF was more effective in the monosaccharide conversion than water and alcohols (e.g., methanol, ethanol, and isopropyl alcohol) because of its advantage for mediating the dehydration of fructose by preventing rehydration of 5-HMF to form levulinic acid [12]. Based on the previous results, conversion of disaccharides (sucrose and cellobiose) and polysaccharides (starch and cellulose) into 2,5-DMF herein was carried out in THF. Because 5-HMF is the reaction intermediate required to produce 2,5-DMF, the disaccharide and polysaccharide conversion should be carried out over effective acid catalysts. Consecutive reactions of glycosidic bond cleavage by acidolysis of di- and polysaccharides will proceed to produce glucose, isomerization of glucose to produce fructose, and dehydration of fructose to produce 5-HMF. Previous works showed that some solid acid catalysts (e.g. zeolites, SiO₂-Al₂O₃, and WO₃/ZrO₂), which contained both Brønsted and Lewis acid sites, initiated glycosidic bond cleavage, isomerization, and dehydration reaction [47,48]. Therefore, in this section, the feasibility of using the UiO-66(NH₂)@SGO support for the conversion of di- and polysaccharides was tested.

As discussed in the previous section, SGO contained the Brønsted acid site and UiO-66(NH₂) contained both the Brønsted acid and Lewis acid sites. Therefore, the ratio of Brønsted and Lewis acidity in the US supports can be controlled by adjusting the composition of UiO-66(NH₂) and SGO in the US support. To find an optimum ratio of UiO-66(NH₂) and SGO in the US support, the activity of the metal-free US supports with different UiO-66(NH₂):SGO ratios was tested during sucrose conversion at 200 °C and an initial H₂ pressure of 1 MPa for 3 h. As shown in Fig. 8a, when SGO (S₁₀₀) was used, the sucrose conversion was 63.2% and the yields of 5-HMF and FA were 21.7% and 14.5%, respectively. This indicates α-Glc(1 → 2)β-Fru glycosidic bond cleavage by acidolysis and the subsequent dehydration of the produced fructose into 5-HMF over the Brønsted acid site in SGO. A schematic of the sucrose conversion over S₁₀₀ is shown in Fig. 8b. As shown in the GC-TOF/MS chromatogram of the reaction mixture produced over S₁₀₀ (Fig. S7b), the major products of sucrose conversion were FA and 5-HMF, while the minor products included anhydrous sugars (levoglucosenone, #2; 1,4:3,6-dianhydro-α-glucopyranose, #3; levoglucosan, #6) and linear C6 (d-allose, #5). The anhydrous sugars were produced by the dehydration of glucose. The formation of d-allose was caused by the ring opening of fructose over the strong Brønsted acid sites associated with the sulfonated group (-SO₃H) in SGO. The produced d-allose can then undergo C–C cleavage to form FA [49]. The chemical species that were produced over S₁₀₀ are different from those produced in the

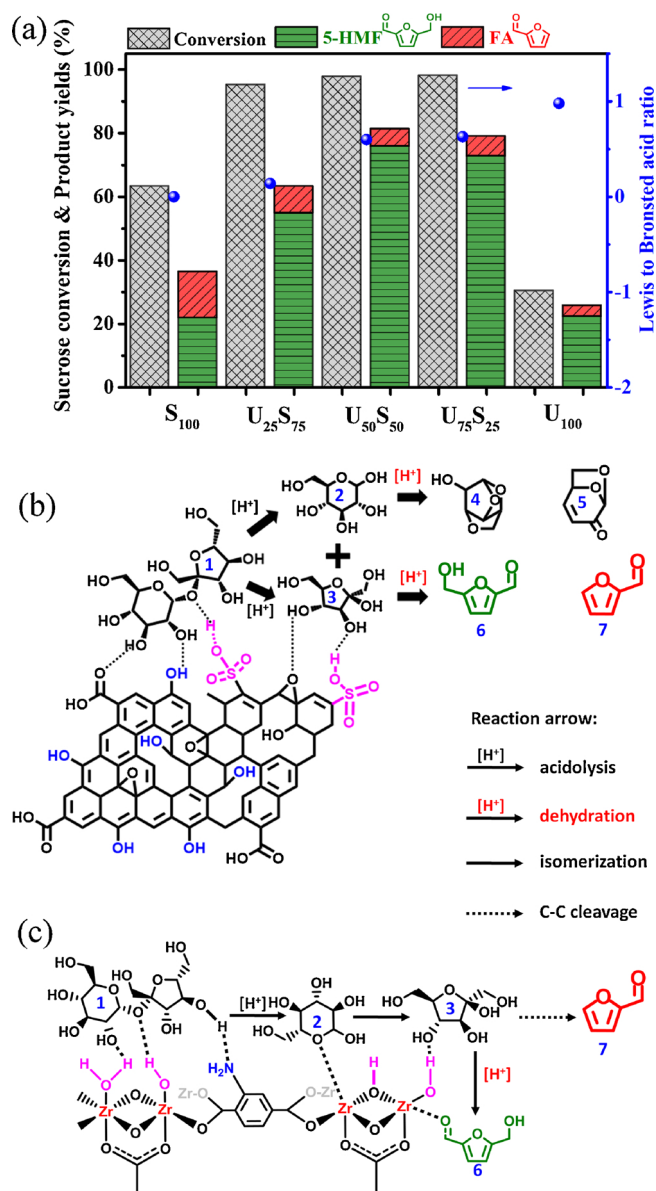


Fig. 8. (a) Sucrose conversion over SGO (S₁₀₀), UiO-66(NH₂) (U₁₀₀), and the US support with various UiO-66(NH₂): SGO ratios including U₂₅S₇₅ (UiO-66(NH₂): SGO = 25:75); U₅₀S₅₀ (UiO-66(NH₂): SGO = 50:50); and U₇₅S₂₅ (UiO-66(NH₂): SGO = 75:25) and their corresponding Lewis to Brønsted acid ratio determined by Py-FTIR. (b) Plausible sucrose conversion mechanisms over S₁₀₀, and (c) plausible sucrose conversion mechanisms over U₁₀₀. (1) sucrose, (2) glucose, (3) fructose, (4) 1,4:3,6-dianhydro- α -D-glucopyranose, (5) levoglucosenone, (6) 5-HMF, and (7) FA. Reaction conditions: 1 mmol of sucrose, an equivalent weight of feed to catalyst ratio, 40 mL THF, and 1 MPa H₂ at 200 °C for 3 h.

absence of catalyst (Fig. S7a), indicating important role of the catalyst for selective chemical production. To check the possibility of converting glucose directly into 5-HMF, glucose was converted over SGO, and the result is shown in Fig. S7c. The products included anhydrous sugars (levoglucosenone, #2; 1,4:3,6-dianhydro- α -glucopyranose, #3), but 5-HMF was not detected. This suggests that the glucose produced by acidolysis of sucrose undergoes a dehydration reaction if it remained un-isomerized into fructose because of the absence of a Lewis acid site in SGO. This indicates that only the fructose part in sucrose contributed to produce 5-HMF over SGO, while the glucose part in sucrose formed anhydrous sugars.

In contrast to S₁₀₀, the sucrose reaction over U₁₀₀ resulted in a significantly low conversion of 30.2% and a low FA yield of 3.5%

(Fig. 8a and S7d). On the other hand, the 5-HMF yield was majorly obtained (22.1%). The low sucrose conversion is due to the large molecular size of sucrose (0.92 nm) [50], which is much larger than the measured micropore size of UiO-66(NH₂) (0.7 nm). Thus, the large-size sucrose molecule could not be effectively transported into the Brønsted acid site in UiO-66(NH₂). The high 5-HMF yield was caused by the high Brønsted acidity sites in UiO-66(NH₂). As discussed previously, HCl-modulated synthesis of UiO-66(NH₂) had Brønsted acidic sites, as shown by the presence of acidic protons (2.03 mmol g⁻¹, Table 2). The acidic proton has originated from the Zr(IV)- μ 3-OH, Zr(IV)-OH, and Zr(IV)-H₂O species in the UiO-66(NH₂) structure [51]. Therefore, UiO-66(NH₂) can facilitate the dehydration of fructose into 5-HMF in the absence of the -SO₃H group, as shown in Fig. 8c. In addition, the dominant production of 5-HMF over FA in the presence of U₁₀₀ is due to the Lewis acid sites associated with the Zr⁴⁺ node inside the UiO-66(NH₂) framework structure, as evidenced by Py-FTIR (Fig. 7a). The Lewis active sites play a role in the isomerization of glucose into fructose, and thus subsequent dehydration of fructose produces additional 5-HMF [52].

The sucrose conversion and 5-HMF yield significantly increased when the US supports with different UiO-66(NH₂) and SGO ratios were used as catalysts (Fig. 8a). This is due to the synergetic effect of Brønsted acid sites (-SO₃H groups in SGO and Zr(IV)-OH species in UiO-66(NH₂)) and Lewis acid site (Zr⁴⁺ species in UiO-66(NH₂)) in the US support. In addition, the ratio of UiO-66(NH₂):SGO plays an important role in enhancing the 5-HMF yield, as well as in reducing the formation of undesirable FA. The use of U₂₅S₇₅ with a lower L/B ratio of 0.14 (0.64 mmol g⁻¹ B sites and 0.09 mmol g⁻¹ L sites) resulted in a lower 5-HMF yield as compared to U₇₅S₂₅ with a higher L/B ratio of 0.63 (0.82 mmol g⁻¹ B sites and 0.52 mmol g⁻¹ L sites). When U₅₀S₅₀ with a L/B ratio of 0.60 (1.02 mmol g⁻¹ B sites and 0.61 mmol g⁻¹ L sites) was used, a higher 5-HMF yield of 75.8% and lower FA yield of 5.5% than those produced using U₂₅S₇₅, but similar to those from U₇₅S₂₅. This suggests that it is essential to increase the Brønsted and Lewis acid sites and the L/B ratio up to the optimum value for effective glucose isomerization and dehydration of fructose into 5-HMF as well as to enhance the sucrose conversion [47]. Therefore, it is necessary to increase and balance Brønsted and Lewis acidities of the support to proceed the acidolysis of sucrose, isomerization of glucose, and dehydration of fructose to produce high-yield 5-HMF, while simultaneously suppressing the C-C cleavage of fructose to form FA as the byproduct.

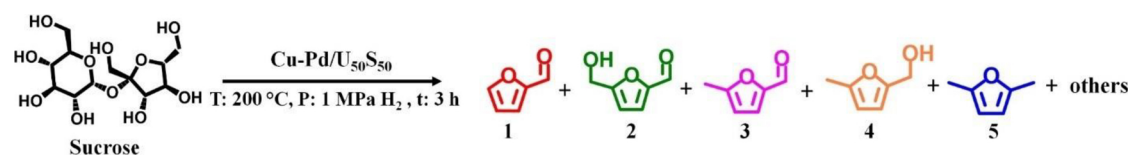
3.2.2. Monometallic Cu-, Pd- and bimetallic Cu-Pd on U₅₀S₅₀

In the previous section, the careful balancing of UiO-66(NH₂) and SGO can form 5-HMF directly from sucrose with high yield. To facilitate hydrogenolysis/hydrogenation of 5-HMF to 2,5-DMF as a part of consecutive sucrose reactions in the one-pot reaction system, it is necessary to choose proper metallic sites that can produce the targeted compound directly by suppressing byproduct formation. In this work, control over the excessive side reactions of 2,5-DMF was attempted, which are typically caused by ring-opening and ring-saturation. To achieve this goal, we investigated bimetallic Cu-Pd as an active material.

To understand the role of bimetallic Cu-Pd as an active site for the consecutive hydrogenolysis/hydrogenation of 5-HMF to 2,5-DMF (Scheme 2), sucrose conversion over the monometallic Cu/U₅₀S₅₀ and Pd/U₅₀S₅₀ catalysts was compared with sucrose conversion over the bimetallic Cu-Pd/U₅₀S₅₀ catalysts at 200 °C and an initial H₂ pressure of 1 MPa for 3 h. As listed in entries 2–4 of Table 3, monometallic Cu/U₅₀S₅₀ catalysts with Cu loadings of 5–15 wt% exhibited moderate activities towards direct sucrose conversion into 2,5-DMF. The U₅₀S₅₀ support plays a role in producing monosaccharides (glucose and fructose) from sucrose through the α -glc(1 \rightarrow 2) β -fru-glycosidic bond cleavage over the Brønsted acid sites, which further isomerized and dehydrated to form 5-HMF. The high Cu loading covers a large surface area of the U₅₀S₅₀ support and suppresses proton donation by the U₅₀S₅₀ support, resulting in decreasing sucrose conversion; as listed in

Table 3

Conversion of cellulosic-based feedstock model compound with Cu- and/or Pd-supported catalyst



| Entry | Saccharide type | Feed ^a | Catalyst ^c | T (°C) | P _{H2} (MPa) | t (h) | X _{feed} (%) | Y _{product} (%) | | | | | |
|-------|------------------|------------------------|---|--------|-----------------------|-------|-----------------------|--------------------------|------------|------------|------------|--------------|--------|
| | | | | | | | | 1 FA | 2 5-HMF | 3 5-MFA | 4 5-MFM | 5 2,5-DMF | others |
| 1 | Di-saccharides | Sucrose | U ₅₀ S ₅₀ | 200 | 1 | 3 | 97.8 | 5.5 | 75.8 | N.D. | N.D. | N.D. | 16.5 |
| 2 | | Sucrose | 5Cu/U ₅₀ S ₅₀ | 200 | 1 | 3 | 97.2 | 20.8 | 43.0 | 2.7 | trace | 19.0 | 11.6 |
| 3 | | Sucrose | (a) 10Cu/U ₅₀ S ₅₀ (b) 10CuO/U ₅₀ S ₅₀ | 200 | 1 | 3 | 96.0 | 15.5 | 32.4 | 3.4 | 2.7 | 27.3 | 14.8 |
| 4 | | Sucrose | 15Cu/U ₅₀ S ₅₀ | 200 | 1 | 3 | 89.1 | 25.2 | 15.0 | 12.9 | 5.1 | 9.8 | 18.1 |
| 5 | | Sucrose | 1Pd/U ₅₀ S ₅₀ | 200 | 1 | 3 | 97.2 | 5.3 | 3.2 | 14.3 | 1.2 | 48.6 | 24.6 |
| 6 | | Sucrose | (a) 10Cu-1Pd/U ₅₀ S ₅₀ (b) 9Cu-2Pd/U ₅₀ S ₅₀ | 200 | 1 | 3 | 95.0 | 0.5 | trace | 3.0 | trace | 73.4 | 18.1 |
| 7 | Poly-saccharides | Sucrose | 4.8Pd/UiO-66@SGO | 200 | 1 | 3 | 74.0 | trace | trace | 25.2 | trace | 38.1 | 10.7 |
| 8 | | Cellobiose | 10Cu-1Pd/U ₅₀ S ₅₀ | 200 | 1 | 3 | 90.0 | 0.1 | trace | 2.3 | 0.3 | 67.7 | 19.6 |
| 9 | | Cellobiose | 4.8Pd/UiO-66@SGO | 200 | 1 | 3 | 69.0 | trace | 5.4 | 32.0 | trace | 29.0 | 2.6 |
| 10 | | Starch | 10Cu-1Pd/U ₅₀ S ₅₀ | 200 | 1 | 6 | 70.0 | trace | trace | trace | 0.4 | 53.6 | 16.1 |
| 11 | | Starch | 4.8Pd/UiO-66@SGO | 200 | 1 | 6 | 53.0 | 5.0 | 8.2 | 10.0 | trace | 19.5 | 10.3 |
| 12 | | Cellulose ^b | 10Cu-1Pd/U ₅₀ S ₅₀ + HCl ^d | 200 | 1 | 6 | 59.0 | 4.3 | 3.1 | 2.1 | trace | 29.8 | 19.7 |
| 13 | Mono-saccharides | Cellulose ^b | 4.8Pd/UiO-66@SGO + HCl ^d | 200 | 1 | 6 | 26.0 | trace | trace | trace | trace | 10.3 | 16.3 |
| 14 | | Fructose | 10Cu-1Pd/U ₅₀ S ₅₀ | 200 | 1 | 3 | 98.0 | 0.8 | 0.1 | 3.2 | trace | 85.1 | 8.88 |
| 15 | | Glucose | 10Cu-1Pd/U ₅₀ S ₅₀ | 200 | 1 | 3 | 97.0 | 0.8 | 0.3 | 3.1 | trace | 79.9 | 12.9 |

^a 1 mmol of feed.^b 0.1 g of cellulose.^c an equimolar weight of feed to catalyst ratio.^d 500 μ L HCl (0.01 M).

Table 2, proton concentrations in the Cu/U₅₀S₅₀ catalysts decreased from 2.50 to 2.38 mmol g⁻¹ as Cu loading increased from 5 to 15 wt%. This supports the important role of the Brønsted acid sites of the U₅₀S₅₀ support in the initial acidolysis of sucrose.

As compared to the U₅₀S₅₀ support (**Table 3**, entry 1), the presence of Cu on U₅₀S₅₀ can coax hydrogenolysis and hydrogenation of 5-HMF to produce 2,5-DMF directly, but the 2,5-DMF yields were low (entries 2–4). As the Cu loading increased from 5 to 15 wt%, the sucrose conversion decreased from 97.2% to 89.1%, and the 2,5-DMF yield decreased from 19.0% to 9.8%. The detrimental effect of a high Cu-loaded catalyst up to 15 wt% on the sucrose conversion and 2,5-DMF yield was caused by the low proton concentration (**Table 2**) and the low specific surface area (**Table 1**) due to the excess deposition of Cu phases on the U₅₀S₅₀ support blocks some of active sites of the U₅₀S₅₀ support. The presence of 5-MFA and 5-MFM in the reaction mixture (entries 2 and 3a) over 5Cu/U₅₀S₅₀ and 10Cu/U₅₀S₅₀ suggest the hydrogenation activity of the Cu⁺/Cu⁰ species to converts the carbonyl group (C=O) in 5-MFA to hydroxyl group (C–OH) in 5-MFM. This is followed by the hydrogenolysis activity of the Cu⁺/Cu⁰ species to convert the C–OH group in 5-MFM [53], which could be responsible for the formation of 2,5-DMF over monometallic Cu catalysts. On the other hand, the residual amounts of unconverted 5-HMF in the reaction mixture were high (15.0–43.0%). The relatively high yield of 5-HMF was caused by the low hydrogenolysis activity of the Cu catalysts to convert the C–OH group in 5-HMF into 5-MFA. This indicates the hydrogenolysis of 5-HMF is the limiting step, as shown in **Fig. 9a** (i). The low C–OH hydrogenolysis activity of 5-HMF on the monometallic Cu/U₅₀S₅₀ catalysts can be caused by preferable C–C cleavage activity of glucose occurred under the temperature condition (200 °C). The high C–C cleavage activity of glucose associated with the monometallic Cu catalyst [54] can result in the formation of undesirable FA (15.5–25.2%) with high yields, which is produced by the C–C cleavage of *d*-allose [49]. Water produced during the hydrogenation at high temperature over the Cu catalyst can also inhibit the C–O hydrogenolysis [55]. In

addition, FA was further hydrogenated into furfuryl alcohol (FOL) in the presence of a Cu catalyst (**Fig. S8b-d**), indicating FA hydrogenation occurred over the Cu catalyst [55]. To clarify the active sites of the Cu catalyst (metallic Cu or Cu oxide), 10CuO/U₅₀S₅₀ was tested in the sucrose conversion, as listed in entry 3b. A much higher amount of 5-HMF (54.3%) remained unconverted as compared to that of 10Cu/U₅₀S₅₀ (32.4%), suggesting that the presence of CuO inhibits the hydrogenolysis activity.

Tests with 1Pd/U₅₀S₅₀ resulted in much higher sucrose conversion of 97.2% with a higher 2,5-DMF yield of 48.6% and a lower FA yield of 5.3% (entry 5, **Table 3**) with a TOF_{Pd} of 32.34 mol_{sucrose}⁻¹ h⁻¹ mol_{Pd}⁻¹ as compared to the Cu/U₅₀S₅₀ catalysts with a TOF_{Cu} 13.14 mol_{sucrose}⁻¹ h⁻¹ mol_{Cu}⁻¹ in case of 10Cu/U₅₀S₅₀. This indicates that Pd is a very effective active phase to direct the hydrogenolysis/hydrogenation/hydrogenolysis of 5-HMF to produce 2,5-DMF. However, a noticeable amount of 5-MFA (14.3%) remained unconverted. This suggests that the hydrogenation of the C=O group in 5-MFA into 5-MFM was the rate-limiting step, as shown in **Fig. 9a** (ii). One of the possible reasons for this phenomena is competitive molecular interaction between C=O group and the π C=C bond in 5-MFA on the surface of Pd(111). Vertical adsorption of the C=O group could be hindered by the horizontal absorption of the π C=C bond tilted on the corresponding Pd(111) surface [56], which suppress the hydrogenation 5-MFA to 5-MFM. In addition, byproducts such as (2,5-DMTHF, #1, **Fig. S11a**) from ring saturation of 2,5-DMF and 2,5-hexanedione (2,5-HDN, #5, **Fig. S11a**) from ring-opening of 2,5-DMF (**Scheme 2**) formed over the 1Pd/U₅₀S₅₀ catalyst, indicating high hydrogenation and ring-opening activity of the Pd catalyst.

As discussed in the previous section, the monometallic Cu/U₅₀S₅₀ catalyst exhibited an excellent hydrogenation activity to convert 5-MFA into 5-MFM and did not result in the side reactions for 2,5-DMF. Meanwhile, the use of monometallic Pd/U₅₀S₅₀ resulted in high hydrogenolysis/hydrogenation/hydrogenolysis activities to produce 2,5-

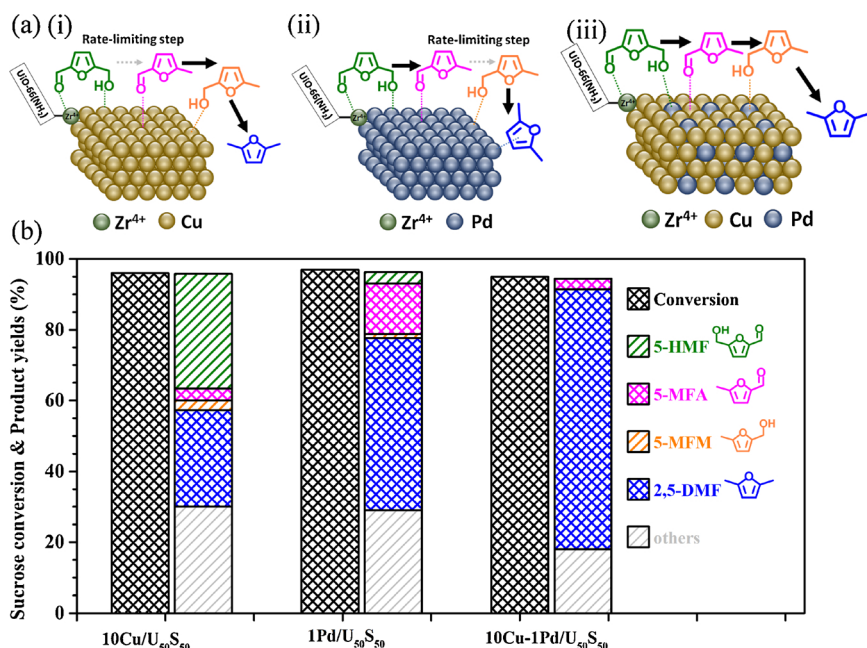


Fig. 9. Sucrose conversion over the monometallic Cu/U₅₀S₅₀ and Pd/U₅₀S₅₀ and the bimetallic Cu-Pd/U₅₀S₅₀ catalysts. (a) Proposed reactions of the 5-HMF transformation on the surface of (i) Cu (111), (ii) Pd (111), and (iii) Cu-Pd, and (b) conversion and product yield of the reaction using 1 mmol of sucrose, an equivalent weight of feed to catalyst ratio, 40 mL THF, and 1 MPa H₂ at 200 °C for 3 h.

DMF with high yield, but the 2,5-DMF side reactions reduced the yield of the target product. Therefore, to maximize the 2,5-DMF yield, bimetallic Cu-Pd/U₅₀S₅₀ catalysts were tested in the sucrose conversion. As listed in entry 6 of Table 3, 10Cu-1Pd/U₅₀S₅₀ had a much higher 2,5-DMF yield of 73.4% with almost complete conversion of the reaction intermediates (5-HMF, 5-MFA, 5-MFM) and suppression of byproduct (FA) formation. This indicates that the rate limiting steps associated with 10Cu/US and 1Pd/US were overcome by combining Cu and Pd in the 10Cu-1Pd/U₅₀S₅₀ catalyst, as shown in Fig. 9a (iii). The other products (Fig. S11d) include 1-hydroxy-2-propanone (#1), 1,2-propanediol (#3), 2,5-dimethyl-2-(1-hydroxy-1-methyl-2-oxopropyl)-3(2H)-furanone (#4), 5-MFA (#6), trace *d*-allose (#7), and 1,6-anhydro- α -D-glucofuranose (#8). We also tested the sucrose conversion with the 4.8Pd/UiO-66@SGO catalyst that was reported in our previous publication [12]. UiO-66 was not amine-functionalized, but a much higher amount of Pd of 4.8 wt% was loaded on the support, as compared to the 10Cu-1Pd/U₅₀S₅₀ catalyst. When fructose was used as the reactant, a high yield of 2,5-DMF (70.5%) resulted over 4.8Pd/UiO-66@SGO [12]. On the other hand, as listed in entry 7 of Table 3, the use of 4.8Pd/UiO-66@SGO resulted in a much lower sucrose conversion of 74.0% and much lower 2,5-DMF yield of 38.1% compared to those with the 10Cu-1Pd/U₅₀S₅₀ catalyst. At least two possible mechanisms could be responsible for the low 2,5-DMF yield from the 4.8Pd/UiO-66@SGO catalyst. First, in the absence of Cu, a large amount of 5-MFA was unconverted over Pd, as evidenced by the high amount of unconverted 5-MFA (25.2%). Second, the amine-functionalized UiO-66(NH₂) plays a role in enhancing sucrose conversion.

To further understand the role of the bimetallic Cu-Pd active phase and its optimum ratio, various amounts of 0.5–2 wt% Pd were incorporated into 10 wt% Cu/U₅₀S₅₀, and the sucrose conversion was tested at 200 °C and an initial H₂ pressure of 1 MPa for various reaction times of 1–3 h. The results are shown in Fig. 10a. As the Pd loading increased from 0.5 to 1 wt%, the 2,5-DMF yield increased significantly from 15.6% to 38.7% during the 1 h reaction. In addition, TOFs increased significantly from 11.68 to 44.11 mol_{sucrose} mol_{Pd}⁻¹ h⁻¹ mol_{sucrose} mol_{Pd}⁻¹ h⁻¹ for the Pd site and from 14.92 to 15.77 mol_{sucrose} mol_{Cu}⁻¹ h⁻¹ mol_{sucrose} mol_{Cu}⁻¹ h⁻¹ for the Cu site (Table S4). A further increase in Pd loading 2 wt% resulted in decreasing 2,5-DMF yield to 29.1%. Although the observed TOF_{Pd} for 10Cu-2Pd/U₅₀S₅₀ was higher (55.25 mol_{sucrose} mol_{Pd}⁻¹ h⁻¹) mol_{sucrose} mol_{Pd}⁻¹ h⁻¹) than that of 10Cu-1Pd/US, TOF_{Cu} was found to be lower (15.09 mol_{sucrose} mol_{Cu}⁻¹ h⁻¹) mol_{sucrose} mol_{Cu}⁻¹ h⁻¹) than that of 10Cu-

1Pd/US. This indicates that an optimum amount of Pd is required to enhance hydrogenolysis of 5-HMF into 5-MFA, while an excessive amount of Pd can result in side reactions to form 2,5-DMTHF from ring saturation of 2,5-DMF and 2,5-hexanedione (HDN) from ring-opening of 2,5-DMF (see Fig. S12). The 5-HMF yield significantly decreased from 20.7% to trace levels as the Pd loading increased from 0.5% to 2.0 wt% indicating that 5-HMF was predominantly converted into its corresponding hydrogenated product of 5-MFA (4.1% to 14.4%) over Pd. This suggests that the high Pd loading can enhance the hydrogenolysis activity of 5-HMF to form 5-MFA. As the reaction time increased to 2 h, more reaction intermediates (5-HMF, 5-MFA, 5-MFM) were converted into 2,5-DMF compared to the 1 h reaction results. The use of 10Cu-1Pd/U₅₀S₅₀ catalyst resulted in a high 2,5-DMF yield of 64.9% during the 2 h reaction. A further increase in reaction time up to 3 h resulted in increasing the 2,5-DMF yield over each Cu-Pd/U₅₀S₅₀ catalyst. The highest 2,5-DMF yield of 73.4% was obtained over the 10Cu-1Pd/U₅₀S₅₀ catalyst. Maintaining the total metal content similar to 10Cu-1Pd/U₅₀S₅₀ catalyst, the lower Cu/Pd ratio in a 9Cu-2Pd/U₅₀S₅₀ catalyst were used for sucrose conversion to check the effect of combined-bimetallic Cu-Pd active phase on the catalyst performance. As listed in entry 6b of Table 3, the use of 9Cu-2Pd/U₅₀S₅₀ resulted in higher 2,5-DMF yield (68%) than that of 10Cu-2Pd/U₅₀S₅₀ (60%). This suggests that optimum total metal content may induced more confined Cu-Pd active phases, resulting the better catalyst activity for producing 2,5-DMF.

The effect of the reaction temperature on sucrose conversion and product yields over the 10Cu-1Pd/U₅₀S₅₀ catalyst was also investigated. As shown in Fig. 10b, when the reaction temperature increased from the 120 to 200 °C for 3 h reaction time, the sucrose conversion and the 2,5-DMF yield increased from 10.6% to 95.0% and from 2.9% to 73.4%, respectively. Based on the Arrhenius equation, the activation energy for the sucrose conversion was calculated to be 83.6 kJ mol⁻¹. This value is much lower than that without any catalyst (300.4 kJ mol⁻¹) [57], but higher than that obtained in the presence of a homogeneous acid catalyst (acetic acid, 42.3 kJ mol⁻¹) [58]. At a low temperature of 120–140 °C, reaction intermediates and byproducts included anhydrosugars, 5-MFA, 5-MFM, and FA, as shown in Fig. S13. This result indicates that in the low temperature regime, sucrose was initially degraded through α -glc(1 \rightarrow 2) β -fru-glycosidic bond cleavage to produce glucose and fructose. Afterwards, the isomerization and dehydration of the corresponding monosaccharides (glucose and fructose) was followed by sequential hydrogenation and hydrogenolysis of 5-HMF, 5-MFA, and 5-MFM to produce 2,5-DMF. As the temperature increased

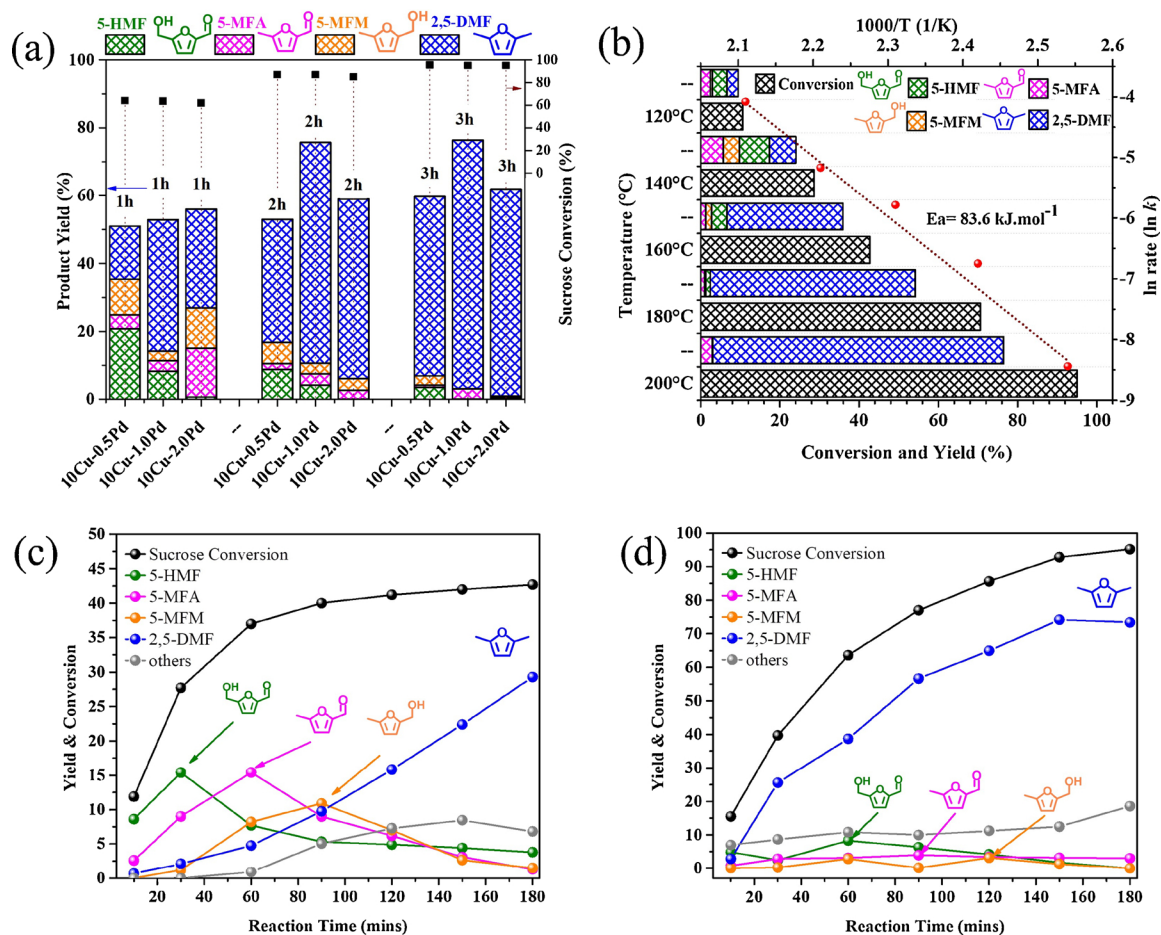


Fig. 10. (a) Sucrose conversion and product yields over 10Cu-0.5Pd/U₅₀S₅₀, 10Cu-1Pd/U₅₀S₅₀, and 10Cu-2Pd/U₅₀S₅₀ catalysts. Reaction conditions: 1 mmol of sucrose, an equivalent weight of feed to catalyst ratio, 40 mL THF, and 1 MPa H₂ from 1 to 3 h at 200 °C. (b) Temperature profiles and Arrhenius plot of sucrose conversion over 10Cu-1Pd/U₅₀S₅₀ at 120–200 °C for 3 h. (c) Time course of reactions at 200 °C and (d) at 160 °C for the sucrose conversion over 10Cu-1Pd/U₅₀S₅₀ at 10–180 min. Reaction conditions: 1 mmol of sucrose, an equivalent weight of feed to catalyst ratio, 40 mL THF, and 1 MPa H₂.

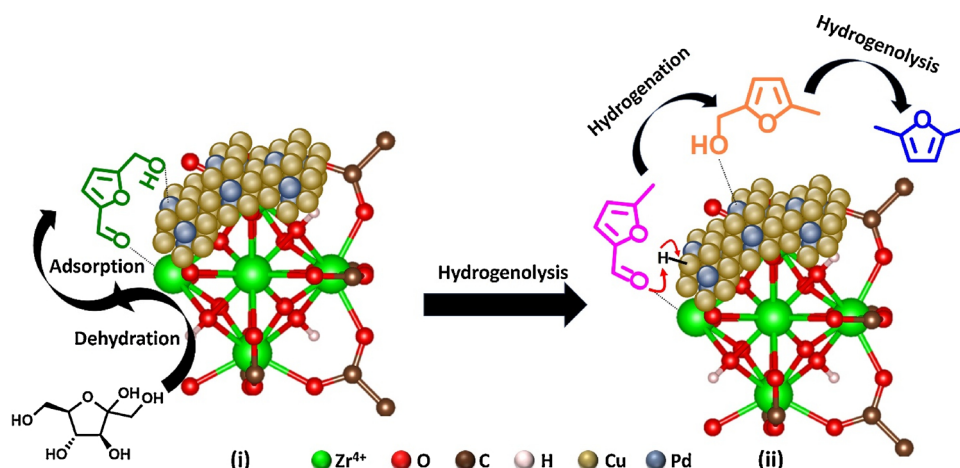
from 160 to 200 °C, only a trace amount of 1,6-anhydro- α -D-glucopyranose was detected, while anhydro- α -D-glucopyranose were not observed, as shown in Fig. S11d.

To explore the reaction pathway of sucrose conversion into 2,5-DMF, the sucrose conversion kinetics at 160 and 200 °C over 10Cu-1Pd/U₅₀S₅₀ from 10 to 180 min under a 1 MPa H₂ was tested, and the reaction data are shown in Fig. 10c–d. The GC-TOF/MS chromatograms of the reaction mixtures at 200 °C were shown in Fig. S11h. At 160 °C in the first 10 min, 11.9% sucrose was converted into products including 8.6% 5-HMF, 2.6% 5-MFA, and trace amount of 5-MFM and 2,5-DMF. As the reaction was further proceeded from 30 to 180 min, the sucrose conversion gradually increased from 37.0% to 42.0%. The 5-HMF yield increased to 15.4% during the first 30 min reaction time, then subsequently decreased into 3.8% as the reaction time was further increased to 180 min. Along with the decrease in 5-HMF, the amount of 5-MFA increased from 2.6% to a maximum point of 15.42% as the reaction time increased from 10 to 60 min and gradually decreased to 1.3% after 180 min. The amounts of 5-MFM were increased slowly in the first 90 min up to 10.9% then gradually decreased to a trace amount for the rest 180 min. At the initial 90 min, a low amount of 2,5-DMF was produced at 160 °C, afterwards it slowly increased to 9.8% followed by rapid increment from 15.8% to 29.3% after 120 to 180 min reaction time. At the high temperature of 200 °C, the produced intermediate species decreased accordingly followed by steady increase of 2,5-DMF from 38.7% to 73.4% after 60 to 180 min reaction time. The time-course of reaction data were in a good agreement with the reaction mechanism proposed in Scheme 2.

3.3. Other feedstock conversion over Cu-Pd/U₅₀S₅₀

When the cellobiose was converted over 10Cu-1Pd/U₅₀S₅₀ catalyst at 200 °C and 1 MPa H₂ for 3 h, the conversion was 90.0% and the 2,5-DMF yield was 67.7% (entry 8, Table 3). These values are slightly lower than those obtained from sucrose (95.0% conversion and 73.4% yield of 2,5-DMF), which can be caused by the stability of β (1 \rightarrow 4) glycosidic bond in cellobiose as compared with that of α -Glc(1 \rightarrow 2) β -Fru in sucrose [59] and the additional isomerization required to produce fructose [52]. As is the case in sucrose conversion, the 10Cu-1Pd/U₅₀S₅₀ catalyst outperformed 4.8Pd/U₅₀S₅₀@SGO in the cellobiose conversion (entry 9, Table 3). When the 10Cu-1Pd/US catalyst was used, trace amounts of reaction intermediates (5-HMF, 5-MFA, 5-MFM) and by-product (FA) formed, while the use of 4.8Pd/U₅₀S₅₀@SGO resulted in 5.4% and 32.0% unconverted 5-HMF and 5-MFA, respectively. When starch was used as the feedstock, 70.0% conversion and 53.6% 2,5-DMF yield were achieved over the 10Cu-1Pd/U₅₀S₅₀ catalyst. Again, the use of 4.8Pd/U₅₀S₅₀@SGO resulted in much lower starch conversion to 2,5-DMF (19.5%) compared to the 10Cu-1Pd/U₅₀S₅₀ catalyst.

Finally, the possibility of cellulose conversion over the 10Cu-1Pd/U₅₀S₅₀ catalyst was tested. At 200 °C and 1 MPa H₂ for 3 h, a negligible amount of cellulose was converted. Therefore, 0.01 M of HCl was added to the reaction mixture to enhance acidolysis of β (1 \rightarrow 4) glycosidic bond cleavage. As listed in entry 12 of Table 3, 59.0% of cellulose conversion and 29.8% 2,5-DMF yield was obtained. Meanwhile, only 26.0% cellulose conversion and 10.3% 2,5-DMF yield resulted over the 4.8Pd/U₅₀S₅₀@SGO catalyst. This indicates the importance of amine-



Scheme 3. Plausible transformation of 5-HMF into 2,5-DMF over the bimetallic Cu-Pd/US catalyst. (i) sequential fructose dehydration into 5-HMF and direct adsorption of 5-HMF onto the adjacent Cu-Pd metallic phase and (ii) sequential hydrogenation of 5-MFA into 5-MFM and hydrogenolysis of 5-MFM into 2,5-DMF.

functionalized UiO-66 and the synergistic effect of the metallic Cu-Pd active phase during cellulose conversion. As discussed in the introduction section, the direct one-pot conversion of fructose over heterogeneous catalysts resulted in 33–88% 2,5-DMF yields [4,12,18]. However, a low 2,5-DMF yield of 45.3% resulted when glucose was used as a feedstock [12]. Herein, the one-pot conversion of fructose and glucose over 10Cu-1Pd/UiO-66 was tested, and the results are listed in entries 14 and 15 of Table 3. High 2,5-DMF yields of 85.1% and 79.9% were obtained from fructose and glucose, respectively, over the 10Cu-1Pd/UiO-66 catalyst, indicating the high activity of the bimetallic Cu-Pd on UiO-66(NH₂).

3.4. Mechanistic insight of one-pot consecutive reaction of sucrose to 2,5-DMF

As discussed in the previous section, the 10Cu-1Pd/UiO-66 catalyst showed high activity on the conversion of monosaccharides and disaccharides into 2,5-DMF, while a relatively low 2,5-DMF yield was obtained when starch was used as the feedstock. Scheme 2 shows the whole reaction pathway of sucrose conversion into 2,5-DMF. Starch and disaccharide depolymerization occurred in the presence of Brønsted acid sites through $\alpha(1 \rightarrow 6)$ and $\alpha\text{-Glc}(1 \rightarrow 2)\beta\text{-Fru}$ or $\beta(1 \rightarrow 4)$ -glycosidic bond cleavage, respectively, which are available in both SGO and UiO-66(NH₂). The isomerization of glucose into fructose proceeds at Lewis acid sites of Zr⁴⁺ present in UiO-66(NH₂). The dehydration of fructose into 5-HMF subsequently occurs in the Brønsted acid sites of SGO and UiO-66(NH₂). Then 5-HMF could undergo two different reaction pathways; (i) hydrogenolysis C–OH bond of 5-HMF to form 5-MFA and (ii) hydrogenation C=O group of 5-HMF to form 2,5-BHMF. The presence of 5-MFA in the reaction mixtures (Table 3, Figs. S11–S13) over all the catalysts tested in this study indicates that the mechanism (i) occurred during the conversion of mono-, di- and polysaccharides. Subsequently, 5-MFA is hydrogenated into 5-MFM, which is further converted into 2,5-DMF through C–OH hydrogenolysis of 5-MFM over Cu⁰/Cu⁺ [53] and Pd⁰ [60]. On the other hand, 2,5-BHMF was not observed in the GC-TOF/MS chromatograms obtained under different reaction conditions, implying the pathway (ii) was highly suppressed. As presented in Table S3 and Fig. S15, the Gibbs free energy reaction of 5-HMF transformations calculated by the DFT simulated under a vacuum condition showed that 5-MFA formation had lower free energy reaction (ΔG^0_{DFT} of $-115.21 \text{ kJ mol}^{-1}$) as compared to 2,5-BHMF formation (ΔG^0_{DFT} of $-83.47 \text{ kJ mol}^{-1}$), indicating that hydrogenolysis of 5-HMF were thermodynamically more favorable than the hydrogenation.

As discussed in the previous paper [12], ring-saturation and ring-

opening of 2,5-DMF over the Pd monometallic catalyst decreased the targeted 2,5-DMF yield. When Pd/C was used, selective ring-saturation of 2,5-DMF into 2,5-DMTHF occurred because the horizontal configuration of the C=C bond in a furan ring is more preferable than the vertical configuration through oxygen-site binding on the Pd surface [11,60]. Ring-opening of 2,5-DMF over Pd/C resulted in the production of 2-hexanone and 2-hexanol [11]. Unlike Pd/C, 10Cu-1Pd/UiO-66 resulted in remarkable 2,5-DMF yield with negligible amounts of ring-saturated and ring-opened side products (Fig. S11b–f). At least two key factors could be responsible for the controlled formation of 2,5-DMF over 10Cu-1Pd/UiO-66. First, MOFs play an important role in selective hydrogenation of compounds containing an α,β -unsaturated aldehyde group [61,62]. Zhao et al. reported the observation of preferential interaction of the C=O aldehyde group of α,β -unsaturated aldehyde model compounds with the unsaturated metal node center over the C–OH group [62]. Similarly, the unsaturated Zr⁴⁺ node centers of UiO-66(NH₂) could prefer to bind the C=O group in 5-HMF, and the C–OH group in 5-HMF could be removed first by hydrogenolysis over the Cu-Pd sites to form 5-MFA (Scheme 3). Then the remaining C=O group in 5-MFA could be hydrogenated over the Cu-Pd sites to form 5-MFM, which can further proceed to form 2,5-DMF by hydrogenolysis of the C–OH group. The produced 2,5-DMF could easily desorb from the catalyst surface due to the absence of C=O and C–OH groups, as these functional groups prefer to interact with the node center in UiO-66(NH₂). Second, the Cu₃Pd atomic crystalline arrangement (Fig. 6) could lead to unfavorable interactions between C=C bonds in 2,5-DMF with the Cu (111) surface and the Cu₃Pd phases. This can suppress the ring saturation and ring opening reactions. In previous papers, Cu preferred to interact with C–OH and C=O groups attached to furanic rings [53,63]. Although the C=C bond interaction could be expected on the adjacent surface of Pd (111), the dominant Cu loading over Pd could reduce the possibility of side reactions. Third, the role of amino-functionalized UiO-66(NH₂) can be responsible for enhancing the catalytic activity towards the hydrophilic substrates (sugars and 5-HMF) because of close contact with the active sites (acidic and metallic sites) [64] in the catalysts compared with the unmodified UiO-66. The simulation of 5-HMF adsorption on the surface of isolated UiO-66 and UiO-66(NH₂) nodes was performed to understand the thermodynamically preferable interaction behaviors. As listed in Table S2 and shown Fig. S14, the DFT calculation of binding energy in the UiO-66(NH₂)-5-HMF system ($-106.41 \text{ kJ mol}^{-1}$) is two-times lower than that of UiO-66-5-HMF system ($-48.01 \text{ kJ mol}^{-1}$). This indicates that the 5-HMF molecule is more thermodynamically preferable to be adsorbed on the UiO-66(NH₂) as compared with UiO-66.

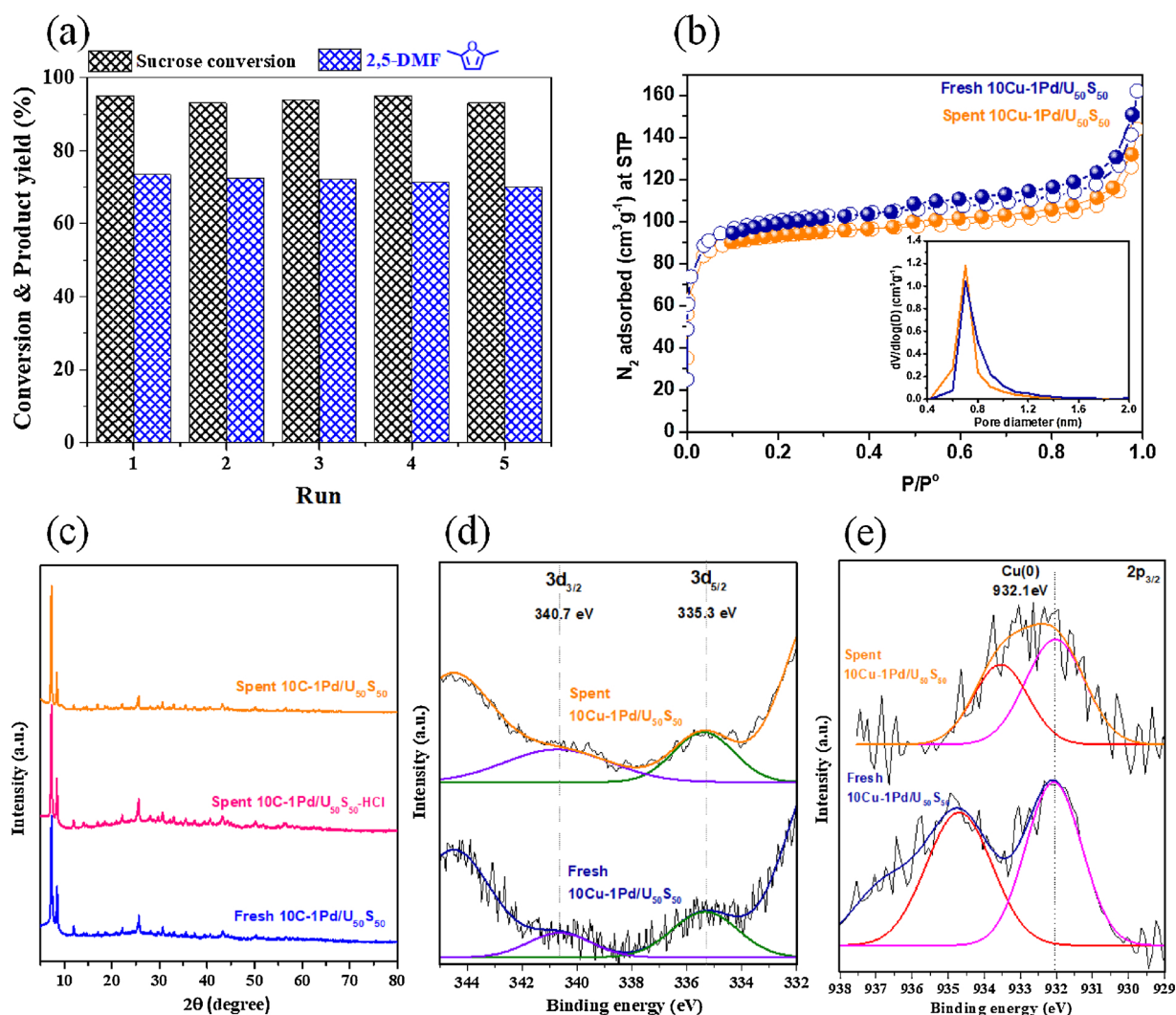


Fig. 11. (a) Recyclability test of the 10Cu-1Pd/U₅₀S₅₀ catalyst. Reaction conditions: 1 mmol sucrose, an equivalent weight of feed to catalyst ratio, 40 mL THF, 200 °C, and 1 MPa of initial H₂ pressure for 3 h. Characterization of spent catalyst 10Cu-1Pd/U₅₀S₅₀ after the five runs. (b) N₂ adsorption–desorption isotherms and micropore (MP) plots, (c) XRD patterns, (d) XPS of core-level Pd 3d spectra and (e) XPS of core-level Cu 2p spectra of the fresh and the spent 10Cu-1Pd/U₅₀S₅₀ catalyst.

3.5. Catalyst reusability

The reusability of the 10Cu-1Pd/U₅₀S₅₀ catalyst was investigated for sucrose conversion in five consecutive test cycles at 200 °C and an initial 1 MPa H₂ for 3 h. The catalyst was initially washed with acetone, ethanol, and water to remove the residual organic-soluble and water-soluble products that could remain on the catalyst. The recycling experiment shown in Fig. 11a indicated that the 10Cu-1Pd/U₅₀S₅₀ catalyst could be reused up to five times with almost stable activity in sucrose conversion and 2,5-DMF yield. As listed in Table 1, Cu and Pd metal contents in the spent 10Cu-1Pd/U₅₀S₅₀ catalyst only slightly decreased after the five consecutive reactions than those of the fresh catalyst, indicating the metal leaching was negligible. The presence of the amine-functionality in UiO-66(NH₂) can prevent the metal leaching [65]. The BET surface area of the spent catalyst (282.3 m² g⁻¹) was slightly lower than that of the fresh catalyst (307.4 m² g⁻¹) and the pore size of the spent catalyst was slightly reduced (Fig. 11b). The HR-TEM images of the spent catalyst shown in Figs. S16a–c indicate that the particle size distribution was slightly larger (5 nm) than that of the fresh catalyst (4.5 nm). The SEM-EDS analysis in Fig. S16d–n demonstrated that the elemental distribution components of the spent 10Cu-1Pd/U₅₀S₅₀ catalyst was uniformly dispersed. Furthermore, as shown in

Fig. 11c, the XRD pattern of spent 10Cu-1Pd/U₅₀S₅₀ catalyst was very similar that of fresh 10Cu-1Pd/U₅₀S₅₀ catalyst, indicating the high stability of the catalyst. In addition, the 10Cu-1Pd/U₅₀S₅₀ catalyst used in the cellulose conversion under the acidic condition (0.01 M HCl) maintained its structure after the reaction, indicating high chemical stability under the acidic condition. The core-level XPS spectra of Pd 3d and Cu 2p of the spent 10Cu-1Pd/U₅₀S₅₀ catalyst (Fig. 11d–e) revealed that the metallic states of Cu and Pd were not changed after the reaction, suggesting high stability of the catalyst.

4. Conclusion

In summary, the chemoselective activity of bimetallic Cu-Pd combined with an optimized ratio of Lewis to Brønsted acidity in UiO-66(NH₂)/SGO resulted in the formation of 2,5-DMF with high yield from di- and polysaccharides (sucrose, cellobiose, starch, and cellulose) in a one-pot reaction system without separation of reaction intermediates. Controlling the ratio of Lewis to Brønsted acidity in the UiO-66(NH₂)/SGO support resulted in the formation of 5-HMF with a high yield of 75.8% via sequential glycosidic bond cleavage, isomerization of glucose into fructose, and dehydration of fructose. When sucrose was used as the feedstock, the bimetallic Cu-Pd phase preceded consecutive

hydrogenation/hydrogenolysis/hydrogenation of 5-HMF into 2,5-DMF with a high yield of 73.4% at 200 °C and 1 MPa H₂ for 3 h. On the other hand, the use of monometallic Cu/UiO-66(NH₂)@SGO and Pd/UiO-66(NH₂)@SGO catalysts resulted in low sucrose conversion and 2,5-DMF yield, which were caused by rate-limiting reaction intermediates and side reactions, such as ring opening and ring saturation. The highly efficient tandem catalyst proposed in this study shows a great potential in developing an environmentally benign, one-pot catalytic system for complex biomass conversion with cost-effective and simple operation.

Acknowledgements

This study was supported by a National Research Foundation of Korea (NRF) grant funded by the Korean Government (MSIP) (No. 2016R1D1A1B039340602016R1A2B3008800, 2015H1D3A1066544 and 2016R1D1A1B03934060). Additional support by the Technology Development Program to Solve Climate Changes of the National Research Foundation (NRF) funded by the Ministry of Science, ICT & Future Planning (2017M1A2A2087635) was appreciated.

Appendix A. Supplementary data

Supplementary data associated with this article can be found, in the online version, at <https://doi.org/10.1016/j.apcatb.2018.10.036>.

References

- X. Li, P. Jia, T. Wang, Furfural: a promising platform compound for sustainable production of C₄ and C₅ chemicals, *ACS Catal.* 6 (2016) 7621–7640.
- Y. Hayashi, Pot economy and one-pot synthesis, *Chem. Sci.* 7 (2016) 866–880.
- S. Zhong, R. Daniel, H. Xu, J. Zhang, D. Turner, M.L. Wyszynski, P. Richards, Combustion and emissions of 2, 5-dimethylfuran in a direct-injection spark-ignition engine, *Energy Fuels* 24 (2010) 2891–2899.
- Y. Román-Leshkov, C.J. Barrett, Z.Y. Liu, J.A. Dumesic, Production of dimethylfuran for liquid fuels from biomass-derived carbohydrates, *Nature* 447 (2007) 982–985.
- M.A. Dam E. De Jong J. Van Haveren A. Pukin, Process for the preparation of a benzene derivative U.S. Patent 20140235892 A1 2014.
- S. Tierney, M., Heeney, C., Bailey, W. Zhang, Process for Preparing Substituted Pentacenes, U.S. Patent 20100127220 A1, May 27, 2010.
- B.T. Parr, S.A. Green, H.M. Davies, Rhodium-catalyzed conversion of furans to highly functionalized pyrroles, *J. Am. Chem. Soc.* 135 (2013) 4716–4718.
- H.J. Cho, L. Ren, V. Vattipalli, Y.H. Yeh, N. Gould, B. Xu, R.J. Gorte, R. Lobo, P.J. Dauenhauer, M. Tsapatsis, Renewable p-Xylene from 2, 5-dimethylfuran and ethylene using phosphorus-containing zeolite catalysts, *ChemCatChem* 9 (2017) 398–402.
- I.F. Teixeira, B.T. Lo, P. Kostetsky, M. Stamatakis, L. Ye, C.C. Tang, G. Mpourmpakis, S.C.E. Tsang, From biomass-Derived furans to aromatics with ethanol over zeolite, *Angew. Chem. Int. Ed.* 55 (2016) 13061–13066.
- M.J. Gilkey, A.V. Mironenko, L. Yang, D.G. Vlachos, B. Xu, Insights into the ring-opening of biomass-derived furanics over carbon-supported ruthenium, *ChemSusChem* 9 (2016) 3113–3121.
- Y.L. Louie, J. Tang, A.M. Hell, A.T. Bell, Kinetics of hydrogenation and hydrogenolysis of 2, 5-dimethylfuran over noble metals catalysts under mild conditions, *Appl. Catal. B* 202 (2017) 557–568.
- R. Insyani, D. Verma, S.M. Kim, J. Kim, Direct one-pot conversion of mono-saccharides into high-yield 2, 5-dimethylfuran over a multifunctional Pd/Zr-based metal-organic framework@ sulfonated graphene oxide catalyst, *Green Chem.* 19 (2017) 2482–2490.
- H. Li, W. Zhao, Z. Fang, Hydrophobic Pd nanocatalysts for one-pot and high-yield production of liquid furanic biofuels at low temperatures, *Appl. Catal. B* 215 (2017) 18–27.
- P.P. Upare, D.W. Hwang, Y.K. Hwang, U.-H. Lee, D.-Y. Hong, J.-S. Chang, An integrated process for the production of 2, 5-dimethylfuran from fructose, *Green Chem.* 17 (2015) 3310–3313.
- J.B. Binder, R.T. Raines, Simple chemical transformation of lignocellulosic biomass into furans for fuels and chemicals, *J. Am. Chem. Soc.* 131 (2009) 1979–1985.
- Z. Wei, J. Lou, Z. Li, Y. Liu, One-pot production of 2, 5-dimethylfuran from fructose over Ru/C and a Lewis-Brønsted acid mixture in N, N-dimethylformamide, *Catal. Sci. Technol.* 6 (2016) 6217–6225.
- B. Saha, C.M. Bohn, M.M. Abu-Omar, Zinc-assisted hydrodeoxygenation of biomass-derived 5-hydroxymethylfurfural to 2, 5-dimethylfuran, *ChemSusChem* 7 (2014) 3095–3101.
- H. Li, W. Zhao, A. Riisager, S. Saravanamurugan, Z. Wang, Z. Fang, S. Yang, A Pd-catalyzed in situ domino process for mild and quantitative production of 2, 5-dimethylfuran directly from carbohydrates, *Green Chem.* 19 (2017) 2101–2106.
- S.H. Bhosale, M.B. Rao, V.V. Deshpande, Molecular and industrial aspects of glucose isomerase, *Microbiol. Rev.* 60 (1996) 280–300.
- D.C. Marcano, D.V. Kosynkin, J.M. Berlin, A. Sinitskii, Z. Sun, A. Slesarev, L.B. Alemany, W. Lu, J.M. Tour, Improved synthesis of graphene oxide, *ACS Nano* 4 (2010) 4806–4814.
- Q. Hou, W. Li, M. Ju, L. Liu, Y. Chen, Q. Yang, One-pot synthesis of sulfonated graphene oxide for efficient conversion of fructose into HMF, *RSC Adv.* 6 (2016) 104016–104024.
- M.J. Katz, Z.J. Brown, Y.J. Colón, P.W. Siu, K.A. Scheidt, R.Q. Snurr, J.T. Hupp, O.K. Farha, A facile synthesis of UiO-66, UiO-67 and their derivatives, *Chem. Commun.* 49 (2013) 9449–9451.
- T. Subramanian, K. Pitchumani, Transfer hydrogenation of carbonyl compounds and carbon-carbon multiple bonds by zeolite supported Cu nanoparticles, *Catal. Sci. Technol.* 2 (2012) 296–300.
- H. Prajitno, R. Insyani, J. Park, C. Ryu, J. Kim, Non-catalytic upgrading of fast pyrolysis bio-oil in supercritical ethanol and combustion behavior of the upgraded oil, *Appl. Energy* 172 (2016) 12–22.
- A. Bhan, A.D. Allian, G.J. Sunley, D.J. Law, E. Iglesia, Specificity of sites within eight-membered ring zeolite channels for carbonylation of methyls to acetyls, *J. Am. Chem. Soc.* 129 (2007) 4919–4924.
- T.W. Walker, A.K. Chew, H. Li, B. Demir, Z.C. Zhang, G.W. Huber, R.C. Van Lehn, J.A. Dumesic, Universal kinetic solvent effects in acid-catalyzed reactions of biomass-derived oxygenates, *Energy Environ. Sci.* 11 (2018) 617–628.
- B. Delley, Fast calculation of electrostatics in crystals and large molecules, *J. Phys. Chem.* 100 (1996) 6107–6110.
- J.P. Perdew, K. Burke, M. Ernzerhof, Generalized gradient approximation made simple, *Phys. Rev. Lett.* 77 (1996) 3865.
- A. Tkatchenko, M. Scheffler, Accurate molecular van der Waals interactions from ground-state electron density and free-atom reference data, *Phys. Rev. Lett.* 102 (2009) 073005.
- S. Ma, M. Sadakiyo, M. Heima, R. Luo, R.T. Haasch, J.I. Gold, M. Yamauchi, P.J. Kenis, Electroreduction of carbon dioxide to hydrocarbons using bimetallic Cu-Pd catalysts with different mixing patterns, *J. Am. Chem. Soc.* 139 (2016) 47–50.
- A. Serov, T. Asset, M. Padilla, I. Matanovic, U. Martinez, A. Roy, K. Artyushkova, M. Chatenet, F. Maillard, D. Bayer, Highly-active Pd-Cu electrocatalysts for oxidation of ubiquitous oxygenated fuels, *Appl. Catal. B* 191 (2016) 76–85.
- Z. Xi, J. Li, D. Su, M. Muzzio, C. Yu, Q. Li, S. Sun, Stabilizing CuPd nanoparticles via CuPd coupling to WO₂. 72 nanorods in electrochemical oxidation of formic acid, *J. Am. Chem. Soc.* 139 (2017) 15191–15196.
- L. Valenzano, B. Civalieri, S. Chavan, S. Bordiga, M.H. Nilsen, S. Jakobsen, K.P. Lillerud, C. Lamberti, Disclosing the complex structure of UiO-66 metal organic framework: a synergic combination of experiment and theory, *Chem. Mater.* 23 (2011) 1700–1718.
- M.V. Castegnaro, A. Gorgeski, B. Balke, M.d.C.M. Alves, J. Morais, Charge transfer effects on the chemical reactivity of Pd x Cu 1-x nanoalloys, *Nanoscale* 8 (2016) 641–647.
- Z. Guo, T. Liu, W. Li, C. Zhang, D. Zhang, Z. Pang, Carbon supported oxide-rich Pd-Cu bimetallic electrocatalysts for ethanol electrooxidation in alkaline media enhanced by Cu/CuOx, *Catalysts* 6 (2016) 62.
- S.K. Sengar, B. Mehta, G. Gupta, Charge transfer, lattice distortion, and quantum confinement effects in Pd, Cu, and Pd-Cu nanoparticles; size and alloying induced modifications in binding energy, *Appl. Phys. Lett.* 98 (2011) 193115.
- X. Liu, X. Wang, G. Xu, Q. Liu, X. Mu, H. Liu, Tuning the catalytic selectivity in biomass-derived succinic acid hydrogenation on FeO x-modified Pd catalysts, *J. Mater. Chem. A* 3 (2015) 23560–23569.
- C.-W. Chou, S.-J. Chu, H.-J. Chiang, C.-Y. Huang, C.-j. Lee, S.-R. Sheen, T.P. Perng, C.-t. Yeh, Temperature-programmed reduction study on calcination of nano-palladium, *J. Phys. Chem. B* 105 (2001) 9113–9117.
- M.J. Kelly, J. Kim, G.W. Roberts, H.H. Lamb, Characterization of pd/gamma-Al(2)O(3) catalysts prepared using Pd(hfac)(2) in liquid CO(2), *Top. Catal.* 49 (2008) 178–186.
- J. Xue, X. Wang, G. Qi, J. Wang, M. Shen, W. Li, Characterization of copper species over Cu/SAPO-34 in selective catalytic reduction of NOx with ammonia: relationships between active Cu sites and de-NOx performance at low temperature, *J. Catal.* 297 (2013) 56–64.
- A. Penkova, L.F. Bobadilla, F. Romero-Sarria, M.A. Centeno, J.A. Odriozola, Pyridine adsorption on NiSn/MgO-Al 2 O 3: an FTIR spectroscopic study of surface acidity, *Appl. Surf. Sci.* 317 (2014) 241–251.
- J. Jiang, O.M. Yaghi, Brønsted acidity in metal-organic frameworks, *Chem. Rev.* 115 (2015) 6966–6997.
- C. Racles, M.-F. Zaltariov, M. Iacob, M. Silion, M. Avadanei, A. Barga, Siloxane-based metal-organic frameworks with remarkable catalytic activity in mild environmental photodegradation of azo dyes, *Appl. Catal. B* 205 (2017) 78–92.
- M.R. Mani, R. Chellawamy, Y.N. Marathe, V.K. Pillai, Enhanced nucleation of polypropylene by metal-organic frameworks (MOFs) based on aluminium dicarboxylates: influence of structural features, *RSC Adv.* 6 (2016) 1907–1912.
- J. He, M. Liu, K. Huang, T.W. Walker, C.T. Maravelias, J.A. Dumesic, G.W. Huber, Production of levoglucosone and 5-hydroxymethylfurfural from cellulose in polar aprotic solvent-water mixtures, *Green Chem.* 19 (2017) 3642–3653.
- F. Cao, T.J. Schwartz, D.J. McClelland, S.H. Krishna, J.A. Dumesic, G.W. Huber, Dehydration of cellulose to levoglucosone using polar aprotic solvents, *Energy Environ. Sci.* 8 (2015) 1808–1815.
- S. Saravanamurugan, I. Tosi, K.H. Rasmussen, R.E. Jensen, E. Taarning, S. Meier, A. Riisager, Facile and benign conversion of sucrose to fructose using zeolites with balanced Brønsted and Lewis acidity, *Catal. Sci. Technol.* 7 (2017) 2782–2788.
- R. Weingarten, G.A. Tompsett, W.C. Conner, G.W. Huber, Design of solid acid

- catalysts for aqueous-phase dehydration of carbohydrates: the role of Lewis and Brønsted acid sites, *J. Catal.* 279 (2011) 174–182.
- [49] J. Cui, J. Tan, T. Deng, X. Cui, Y. Zhu, Y. Li, Conversion of carbohydrates to furfural via selective cleavage of the carbon–carbon bond: the cooperative effects of zeolite and solvent, *Green Chem.* 18 (2016) 1619–1624.
- [50] L.E. Ramm, M.B. Whitlow, M.M. Mayer, Transmembrane channel formation by complement: functional analysis of the number of C5b6 C7, C8, and C9 molecules required for a single channel, *Proc. Natl. Acad. Sci. U. S. A.* 79 (1982) 4751–4755.
- [51] C. Caratelli, J. Hajek, F.G. Cirujano, M. Waroquier, F.X.L. i Xamena, V. Van Speybroeck, Nature of active sites on UiO-66 and beneficial influence of water in the catalysis of Fischer esterification, *J. Catal.* 352 (2017) 401–414.
- [52] M. Yabushita, P. Li, T. Islamoglu, H. Kobayashi, A. Fukuoka, O.K. Farha, A. Katz, Selective metal–organic framework catalysis of glucose to 5-hydroxymethylfurfural using phosphate-Modified NU-1000, *Ind. Eng. Chem. Res.* 56 (2017) 7141–7148.
- [53] K.L. Deutsch, B.H. Shanks, Copper mixed metal oxide catalysts in the hydrogenolysis of 5-methylfurfuryl alcohol, *Appl. Catal. A* 470 (2014) 390–397.
- [54] B. Kühne, H. Vogel, R. Meusinger, S. Kunz, M. Kunz, Mechanistic study on–C–O–and–C–C–hydrogenolysis over Cu catalysts: identification of reaction pathways and key intermediates, *Catal. Sci. Technol.* 8 (2018) 755–767.
- [55] S. Sitthisa, T. Sooknoi, Y. Ma, P.B. Balbuena, D.E. Resasco, Kinetics and mechanism of hydrogenation of furfural on Cu/SiO₂ catalysts, *J. Catal.* 277 (2011) 1–13.
- [56] M.S. Ide, B. Hao, M. Neurock, R.J. Davis, Mechanistic insights on the hydrogenation of α , β -unsaturated ketones and aldehydes to unsaturated alcohols over metal catalysts, *ACS Catal.* 2 (2012) 671–683.
- [57] Y. Zhang, C. Liu, X. Chen, Unveiling the initial pyrolytic mechanisms of cellulose by DFT study, *J. Anal. Appl. Pyrol.* 113 (2015) 621–629.
- [58] K.L. Fleming, J. Pfaendtner, Characterizing the catalyzed hydrolysis of β -1, 4 glycosidic bonds using density functional theory, *J. Phys. Chem. A* 117 (2013) 14200–14208.
- [59] R. Wolfenden, Y. Yuan, Rates of spontaneous cleavage of glucose, fructose, sucrose, and trehalose in water, and the catalytic proficiencies of invertase and trehalase, *J. Am. Chem. Soc.* 130 (2008) 7548–7549.
- [60] V. Vorotnikov, G. Mpourmpakis, D.G. Vlachos, DFT study of furfural conversion to furan, furfuryl alcohol, and 2-methylfuran on Pd (111), *ACS Catal.* 2 (2012) 2496–2504.
- [61] Z. Guo, C. Xiao, R.V. Maligal-Ganesh, L. Zhou, T.W. Goh, X. Li, D. Tesfagaber, A. Thiel, W. Huang, Pt nanoclusters confined within metal–organic framework cavities for chemoselective cinnamaldehyde hydrogenation, *ACS Catal.* 4 (2014) 1340–1348.
- [62] M. Zhao, K. Yuan, Y. Wang, G. Li, J. Guo, L. Gu, W. Hu, H. Zhao, Z. Tang, Metal–organic frameworks as selectivity regulators for hydrogenation reactions, *Nature* 539 (2016) 76–80.
- [63] W. Liu, Y. Jiang, K.-H. Dostert, C.P. O'Brien, W. Riedel, A. Savara, S. Schauerermann, A. Tkatchenko, Catalysis beyond frontier molecular orbitals: selectivity in partial hydrogenation of multi-unsaturated hydrocarbons on metal catalysts, *Sci. Adv.* 3 (2017) e1700939.
- [64] J. Hajek, M. Vandichel, B. Van de Voorde, B. Bueken, D. De Vos, M. Waroquier, V. Van Speybroeck, Mechanistic studies of aldol condensations in UiO-66 and UiO-66-NH₂ metal organic frameworks, *J. Catal.* 331 (2015) 1–12.
- [65] L. Chen, H. Chen, R. Luque, Y. Li, Metal-organic framework encapsulated Pd nanoparticles: towards advanced heterogeneous catalysts, *Chem. Sci.* 5 (2014) 3708–3714.